Chemical Speciation of Sulfur in Marine Cloud Droplets and Particles: Analysis of Individual Particles from the Marine Boundary Layer over the California Current.

Yuri Desyaterik[†], Rahul A. Zaveri, Carl M. Berkowitz, and Alexander Laskin*

William R. Wiley Environmental Molecular Sciences Laboratory and
Atmospheric Science and Global Change Division,
Pacific Northwest National Laboratory, Richland, WA 99352, USA

Rebecca J. Hopkins[†], Alexei V. Tivanski, Tolek Tyliszczak, and Mary K. Gilles*

Chemical Sciences Division and Advanced Light Source
Lawrence Berkeley National Laboratory, Berkeley, CA 94720-1460, USA

Manuscript 2007JD008954 - *Journal of Geophysical Research – Atmospheres*,

Submitted - *May, 2007*, Revised - *September, 2007*

[†]Authors contributed equally to this work.

*Authors to whom correspondence should be addressed:.

Alexander Laskin (Alexander.Laskin@pnl.gov)
Mary K. Gilles (MKGilles@lbl.gov)

ABSTRACT

Detailed chemical speciation of the dry residue particles from individual cloud droplets and interstitial aerosol collected during the Marine Stratus Experiment (MASE) was performed using a combination of complementary microanalysis techniques. Techniques include computer controlled scanning electron microscopy with energy dispersed analysis of X-rays (CCSEM/EDX), time-of-flight secondary ionization mass spectrometry (TOF-SIMS), and scanning transmission X-ray microscopy with near edge X-ray absorption fine structure spectroscopy (STXM/NEXAFS). Samples were collected at the ground site located in Point Reyes National Seashore, approximately 1 km from the coast. This manuscript focuses on the analysis of individual particles sampled from air masses that originated over the open ocean and then passed through the area of the California current located along the northern California coast. Based on composition, morphology, and chemical bonding information, two externally mixed, distinct classes of sulfur containing particles were identified: chemically modified (aged) sea salt particles and secondary formed sulfate particles. The results indicate substantial heterogeneous replacement of chloride by methanesulfonate ($CH_3SO_3^-$) and non-sea salt sulfate (nss-SO_4^{2-}) in sea-salt particles with characteristic ratios of nss-S/Na > 0.10 and $CH_3SO_3^-$/nss-SO_4^{2-} > 0.6.

1. INTRODUCTION

Aerosols in the unpolluted marine boundary layer (MBL) result from two major sources. First, sea salt particles generated from wave action, which are typically micrometers or larger in size. Second, acidic sulfate aerosol formed by nucleation, with sizes on the order of tenths of a micrometer. This mixture of particle types evolves with time due to a number of processes, including deposition of condensable species, uptake of gas-phase species and a variety of heterogeneous gas-to-particle and homogenous in-particle chemical reactions. Increased interest in the chemical composition and heterogeneity of marine aerosols stems from their regional and global impact on sulfur oxidation in the MBL, in addition to climate effects arising from light scattering and cloud condensation nuclei (CCN) activity [*Covert, et al.*, 1992; *Gong*, 2003; *Gong and Barrie*, 2003; *Gong, et al.*, 1997; *Gong, et al.*, 2002; *Lewis and Schwartz*, 2004; *Murphy, et al.*, 1998; *Quinn, et al.*, 1993; *Sievering, et al.*, 1991; *Sievering, et al.*, 2004].

The major gaseous precursor for marine sulfur-containing aerosol is dimethyl sulfide (DMS). DMS is produced and emitted into the atmosphere by marine phytoplankton [*Keller, et al.*, 1989]. Current estimates of global emissions indicate that DMS is the largest source of natural sulfur [*Bates, et al.*, 1992; *Kettle, et al.,* 1999], produced at a rate of ~12 Tg S yr^{-1} [*Spiro, et al.*, 1992]. In the atmosphere, DMS undergoes a complex sequence of gas-phase oxidation reactions, producing a wide variety of oxidized products, which in turn interact with marine cloud droplets and aerosols. These interactions include nucleation of new particles and the alteration of pre-existing droplets and aerosols through condensation and multiphase chemistry. Due to its large flux, the atmospheric cycle of DMS significantly impacts the radiative budget over oceans on regional and global scales [*Charlson, et al.*, 1987; *Shaw*, 1983].

The atmospheric chemistry of DMS and its possible impact on aerosols and cloud droplets is the subject of many studies. Understanding its major reactions has been achieved through computer kinetic modeling studies [*Charlson, et al.*, 1987; *Kerminen, et al.*, 1998; *Koga and Tanaka*, 1993; 1996; 1999; *Koga, et al.*, 1991; *Lucas and Prinn*, 2002; 2003; 2005a; b; *Shaw*, 1983; *von Glasow and Crutzen*, 2004; *von Glasow, et al.*, 2002a; b; *Yin, Grosjean, Flagan, et al.*, 1990; *Yin, et al.*, 1986; *Yin, Grosjean and Seinfeld*, 1990; *Zaveri*, 1997], focused laboratory studies [*Arsene, et al.*, 2002; *Barnes, et al.*, 1994; *Barone, et al.*, 1996; *Hynes, et al.*, 1995; *Hynes and Wine*, 1996; *Hynes, et al.*, 1986; *Ravishankara, et al.,* 1997; *Stickel, et al.*, 1992; *Turnipseed, et al.,* 1997; *Urbanski, et al.*, 1998; *Yin, et al.*, 1986; *Zhao, et al.*, 1996; *Zhu, et al.*, 2006; *Zhu, et al.*, 2003], and field observations [*M. O. Andreae and Raemdonck*, 1983; *T. W. Andreae, et al.*, 1993; *Bandy, et al.*, 1992; *Bandy, et al.*, 2002; *Barnard, et al.*, 1982; *Cooper and Saltzman*, 1991; 1993; *Spicer, et al.*, 1996; *Zemmelink, et al.*, 2002]. A simplified schematic diagram illustrating DMS chemistry and its climate links is presented in Figure 1. In the ambient atmosphere, oxidation of DMS is initiated by reaction with a variety of atmospheric free radicals. These radicals include, but are not limited to, OH, NO_3, $O(^3P)$, Cl, Br, and BrO. Such reactions proceed *via* two generalized reaction pathways: either addition of an O atom and/or abstraction of an H atom. The branching ratio between the two generalized pathways is temperature dependent with H abstraction dominating at room temperature, while O addition becomes increasingly important at temperatures below 280 K [*Hynes, et al.*, 1986; *von Glasow and Crutzen*, 2004]. DMS gas phase oxidation products include sulfur dioxide (SO_2), sulfuric acid (H_2SO_4), dimethylsulfoxide (CH_3SOCH_3), methanesulfinic acid ($CH_3S(O)OH$), methanesulfonic acid (CH_3SO_3H, MSA), in addition to other species [*Lucas and Prinn*, 2002; *von Glasow and Crutzen*, 2004; *Yin, Grosjean, Flagan, et al.*, 1990; *Zaveri*, 1997].

Under atmospheric conditions, H_2SO_4 is the only DMS oxidation product that forms new non-sea salt sulfate (nss-SO_4^{2-}) particles (new CCN) that could potentially increase the cloud albedo. All other products condense onto pre-existing particles, primarily sea salt, leading to changes in particle composition and particle size without formation of new CCN. Fewer and larger particles of mixed sea salt/$CH_3SO_3^-$/nss-SO_4^{2-} composition would reduce cloud albedo and increase the wash-out of particles due to collision coalescence, therefore reducing cloud lifetime. Hence, the partitioning between DMS oxidation products in different atmospheric environments may affect the number and size of CCN, which impacts the chemistry-cloud-climate feedback in the marine atmosphere. For the remainder of this work, methanesulfonate and sulfate are referred to as the anions $CH_3SO_3^-$ and SO_4^{2-} respectively, as in our samples they are present in crystalline form. Their cation pairing may include an array of ions typical for sea salt, i.e. Na^+, Mg^{2+}, K^+ and others that are omitted for clarity.

For a specific set of atmospheric conditions, consecutive uptake of the DMS oxidation products onto cloud droplets and their subsequent oxidation in the aqueous phase, results in different partitioning between $CH_3SO_3^-$ and nss-SO_4^{2-}. Kinetic modeling studies of the $CH_3SO_3^-$/nss-SO_4^{2-} partitioning in marine aerosol predict formation of minor amounts of $CH_3SO_3^-$ and favor production of nss-SO_4^{2-} in sea salt particles under a variety of atmospheric conditions [*Hertel, et al.*, 1994; *Kerminen, et al.*, 1998; *Kloster, et al.*, 2006; *Koga and Tanaka*, 1996; 1999; *Lucas and Prinn*, 2002; *Yin, Grosjean, Flagan, et al.*, 1990; *Zaveri*, 1997]. Measured values of $CH_3SO_3^-$/nss-SO_4^{2-} ratios in bulk samples typically span a range from 0.001 (low latitudes) to 0.6 (high latitudes) [*Allen, et al.*, 1997; *Berresheim, et al.*, 1990; *Burgermeister and Georgii*, 1991; *Galloway, et al.*, 1993; *Ganor, et al.*, 2000; *Kouvarakis and Mihalopoulos*, 2002; *Li and Barrie*, 1993; *Li, Barrie and Sirois*, 1993; *Li, Barrie, Talbot, et al.*, 1993;

120 *Li, et al.*, 1996; *Mihalopoulos, et al.*, 1992; *Saltzman, et al.*, 1985; 1986; *Saltzman, et al.*, 1983;
121 *Sciare, et al.*, 2000; *Wylie and deMora*, 1996]. Recent modeling studies indicate that under
122 certain conditions $CH_3SO_3^-$/nss-SO_4^{2-} ratios as high as 1.2 – 3.3 in marine droplets can occur
123 [*von Glasow and Crutzen*, 2004]. Specifically, high $CH_3SO_3^-$/nss-SO_4^{2-} values resulted from
124 model simulations for the cloudy MBL in winter conditions (surface temperature of 3-8°C
125 over the ocean). The authors concluded that these high ratios could result from previously
126 overlooked halogen chemistry that favors production of $CH_3SO_3^-$ under cold cloud
127 scenarios.

128 The high level of detail used in this model was in principle sufficient to distinguish
129 and predict $CH_3SO_3^-$/nss-SO_4^{2-} ratios in droplets and particles of different origin, *i.e.* sea salt
130 *versus* sulfate particles [*von Glasow and Crutzen*, 2004]. However, validation of these
131 calculations requires field or laboratory data with a similar level of specificity. In this
132 manuscript we report results from single particle analysis of dry residues of cloud droplets
133 and interstitial aerosol that provide information on $CH_3SO_3^-$/nss-SO_4^{2-} ratios in individual
134 marine particles for the first time.

135 Samples were collected during the Marine Stratus Experiment (MASE) of July 2005
136 at the Point Reyes National Seashore located north of San Francisco [*MASE*, 2005]
137 (*http://www.asp.bnl.gov/MASE.html*). This field study provided an excellent opportunity to
138 sample marine particles under relatively cold cloudy conditions, which according to the
139 modeling predictions of *von Glasow and Crutzen* [*von Glasow and Crutzen*, 2004], could display
140 elevated $CH_3SO_3^-$/nss-SO_4^{2-} ratios. At the northern coast of California, cold ocean currents
141 produce preferential upwelling, resulting in low ocean temperatures (~10-15° C) even during
142 summer time. In addition, low altitude clouds form and typically shroud this region during
143 the summer months. This region is also an area of phytoplankton bloom, resulting in

efficient DMS production [*Strub, et al.*, 1990; *A. Thomas and Strub*, 2001; *A. C. Thomas and Strub*, 1990]. These factors provide a unique opportunity for field studies of $CH_3SO_3^-$ and nss-SO_4^{2-} partitioning in marine cloud droplets and particles representative of relatively cold marine atmosphere over an area rich in DMS.

The complementary capabilities of three analytical techniques provide complete chemical speciation of the field collected marine particles, with the aim of identifying the chemical forms of particulate sulfur. The three data sets are consistent with one another and indicate enhanced formation of particulate $CH_3SO_3^-$ in sea salt droplets and particles collected during MASE. This unique combination of single-particle measurements enables quantitative assessment of $CH_3SO_3^-$/nss-SO_4^{2-} ratios in individual particles.

2. EXPERIMENTAL

2.1. **Meteorological Conditions and Sample Collection.** Particle samples were collected continuously during the cloudy period between July 6th 17:00 –July 7th 9:00 Pacific Standard time (July 7th 01:00 – 17:00, UTC) on a seashore site within one kilometer of the Pacific Ocean at the Point Reyes National Seashore, N38°5´, W122°57.43´. This site is shrouded in cold clouds much of the time, as illustrated in Figure 2, and is well situated for sampling cloud droplets and aerosols. Figure 2 shows backward trajectory calculations performed using the HYSLPIT model [*Draxler and Rolph*, 2003], that end at the sampling site on July 6, 21:00 PST (red) and July 7, 09:00 PST (blue). The trajectories indicate that during the 36 hours preceding collection, the air mass passed over open areas of the ocean and then along the northern shore of California. Backward trajectories calculated for 5 days prior to collection revealed that the sampled air traveled over the Pacific Ocean and did not enter continental areas in exception to ~1-2 km of the shore area adjacent to the sampling site.

168 Over the time frame of the backward trajectory calculation shown in Figure 2b, the relative
169 humidity was above 78%, the air temperature was 13-16°C and the height of boundary
170 mixing layer was 250-400 meters.

171 During sampling, the cloud/fog droplets and (interstitial) aerosol were first separated
172 using a counter-flow virtual impactor (CVI) [*Ogren, et al.*, 1985] that directs the flow of small
173 (interstitial) particles and relatively large cloud droplets into two different sampling lines: the
174 CVI line for particles (drops) larger than ~5 μm and the aerosol observing system (AOS)
175 line for particles smaller than ~5 μm. The particles were first dried inside the CVI and AOS
176 probe lines, and the resulting dehydrated particles were collected by two compact time
177 resolved aerosol collectors (TRAC) [*Laskin, et al.*, 2006; *Laskin, Iedema, et al.*, 2003] attached
178 to each of the lines. The TRAC is a conventional one stage jet-to-plate impactor that
179 deposits particles on a rotating impaction plate containing pre-arranged substrates. In this
180 study, each substrate was exposed for 12 minutes of sample collection. The effective
181 aerodynamic cut-off size D_{50} of the TRAC is ~0.36 μm. Three different types of substrates
182 were used in this study: (a) Copper 400 mesh TEM grids coated with Carbon Type-B films
183 (Ted Pella, Inc.) for the CCSEM/EDX analysis, (b) silicon wafer chips (Silson Ltd, Inc.) for
184 the TOF-SIMS analysis, and (c) silicon wafer frames with silicon nitride windows (Silson
185 Ltd, Inc.) for the STXM/NEXAFS analysis. After collection, impaction plates with the
186 exposed substrates were sealed and stored pending analysis.

187 In general, particle samples collected on substrates may suffer from some artifacts.
188 These include evaporation of volatile and semi-volatile species during the sampling, storage
189 and then analysis by the applied techniques as well as possible reactions between sampled
190 particles and trace gases entering the impactor. For $CH_3SO_3^-$ and SO_4^{2-} salts, no sampling
191 artifacts due to the volatilization are expected to occur. Artifacts like the potential reactions

192 of SO_2(g), HCI(g) and NO_2(g) with the samples inside the TRAC, could not be quantified.
193 However, their possible impacts were somewhat minimized by drying particles prior to
194 collection which would decrease their reaction kinetics.

195 **2.2. Methods of laboratory analysis.** Detailed characterization of individual
196 particles required multiple techniques. As illustrated below, applications of different
197 analytical methods are interdependent; hence, the information from one method guides
198 subsequent measurements. Three analytical techniques were applied for particle analysis: (a)
199 CCSEM/EDX – for microscopy imaging of particles and quantitative speciation of their
200 elemental composition, (b) TOF-SIMS – for qualitative detection of $CH_3SO_3^-$ and SO_4^{2-}
201 within individual particles, and (c) STXM/NEXAFS – for quantitative speciation of the
202 $CH_3SO_3^-$ to SO_4^{2-} partitioning within individual particles.

203 A FEI XL30 digital field emission gun environmental scanning electron microscope
204 was used in this work. The microscope is equipped with an EDAX PV7761/54 ME X-ray
205 spectrometer (EDAX, Inc) with a Si(Li) detector with an active area of 30 mm^2 and an
206 ATW2 window. In addition to the standard SEM/EDX mode of operation, the instrument
207 can also operate in computer-controlled (CCSEM/EDX) mode for analysis of individual
208 particles. In the CCSEM/EDX mode, selected samples are inspected automatically and
209 individual particles are recognized by an increase in the detector signal above a threshold
210 level. The program then acquires an X-ray spectrum from each detected particle. In this
211 work, particles with an equivalent circle diameter larger than ≥0.35 μm were measured by
212 the software. The X-ray spectra were acquired for 10 s, at a beam current of ~500 pA and an
213 accelerating voltage of 20 kV. Additional details of the CCSEM/EDX approach employed
214 for the analysis of particles deposited onto carbon coated TEM grids can be found in our
215 recent review article [*Laskin, et al.*, 2006] and references therein.

A TRIFT II time-of-flight secondary ion mass spectrometer (TOF-SIMS), (Physical Electronics, Inc.) was used in this work. TOF-SIMS analysis entails impacting a pulsed primary ion beam onto a solid sample in vacuum and collecting secondary ions of one polarity (positive or negative), using a time-of-flight (TOF) mass analyzer. The particles collected on the silicon wafer chips were placed in the sample holder and subject to a $^{69}Ga^{+}$ source of primary ions in high spatial resolution mode. An accelerating voltage of 15 kV was used for spectral measurements and 25 kV for mapping. The dose rate was 9.8×10^{12} ions cm^{-2}. A combination of static and dynamic modes of operation allowed molecular speciation of different forms of sulfur-containing compounds within individual particles.

STXM/NEXAFS measurements were performed at the carbon (C) (280 – 320 eV) and nitrogen (N) (395 – 430 eV) K-absorption edges and at the sulfur (S) (168 – 176 eV) L-absorption edge. STXM instruments at beamlines 5.3.2 (C, N) and 11.0.2. (C, N, S) of the Advanced Light Source of Lawrence Berkeley National Laboratory were used for these experiments. The intensity of X-rays transmitted through the sample at a fixed energy is measured as the sample is raster scanned to record an image. Sequences of images are acquired at closely spaced energies to record a "stack" of images, which is essentially a three-dimensional map in position, energy and transmission. NEXAFS spectra from individual pixels or particular regions of interest on the sample image are extracted from the stack. The absorption through the sample is obtained by converting the signal (Beer-Lambert Law) using the reference flux measured through a sample free region. This mapping of chemical bonding information in individual particles [*Hopkins, Tivanski, Marten, et al.*, 2007; *Tivanski, et al.*, 2007; *Maria, et al.*, 2004; *Russell, et al.*, 2002] allows a quantitative assessment of the apportionment between different molecular forms of the same element, *i.e.* $CH_3SO_3^-$ and SO_4^{2-} in this work. For comparison purposes, particles of reference materials were examined

240 using TOF-SIMS and STXM/NEXAFS, including sodium sulfate (Na_2SO_4) (99.99% pure),
241 sodium methanesulfonate (CH_3SO_3Na) (98% pure) and ammonium sulfate ($(NH_4)_2SO_4$)
242 (99.99% pure) purchased from Sigma-Aldrich.
243

244 ## 3. EXPERIMENTAL RESULTS AND DISCUSSIONS

245 Twelve samples (6 CVI and 6 AOS samples with time intervals of ~1.5-2 hours
246 between them) from the Point Reyes sampling site collected during the cloudy period were
247 analyzed using CCSEM/EDX single particle analysis. Figure 3 shows typical SEM images of
248 CVI and AOS aerosol samples. The upper images depict samples collected on silicon wafer
249 chips, while the magnified bottom images are from samples collected on TEM grid
250 supported films. As seen from the upper images, the spatial distribution of particles is
251 inhomogeneous. Larger particles are concentrated in the central region, directly under the
252 deposition nozzle and smaller particles are scattered widely from this area. Thus, a
253 statistically significant analysis of particles by CCSEM/EDX requires sampling across the
254 deposition spot, as indicated by the rectangles in the images. The elemental composition was
255 analyzed for ~1000 particles in a region of 500 μm × 80 μm across the deposition spot for
256 each tested sample.

257 A brief inspection using manual SEM/EDX analysis indicated two prominent
258 particle classes, characteristic for both the CVI and AOS samples. The particles were mostly
259 either sea salt or sulfur-rich (S-rich) particles. S-rich particles are composed of a mixture of
260 H_2SO_4 and $(NH_4)_2SO_4$, as discussed below. Sea salt particles are easily recognized (Figure 3,
261 bottom panels) as they are typically of super micron size with cubic-shaped NaCl crystals
262 surrounded by irregularly shaped residues of other salts. In contrast, S-rich particles are

263 submicron in size and spherical. Consistent with the schematic of sulfur-aerosol-climate links
264 presented in Figure 1, larger sea salt particles dominate the CVI samples while smaller S-rich
265 particles are more abundant in the AOS samples.

266 In this work, as illustrated in panel (a) of Figure 4, a simple rule-based assignment
267 was used to separate individual particles into three major classes. All particles (~10,000)
268 detected in the CCSEM/EDX analysis of 12 selected samples are combined in a group and
269 then all particles containing sulfur above the threshold level of 0.5 atomic percent (as
270 detected by the EDX analysis) are separated. Next, sulfur containing particles that also
271 contain sodium are assigned into the "sea salt" class, while those containing only S, O, and
272 N are assigned to the "S-rich" class. Particles in the S-rich class are expected to display
273 mixed H_2SO_4 and $(NH_4)_2SO_4$ composition. All remaining particles are assigned to one, non-
274 specific class of "other" particles. Panel (b) of Figure 4 illustrates the results of this
275 classification scheme for particles sampled from the CVI and AOS lines over the cloudy
276 period studied here. In general, significant populations of sea salt particles dominate samples
277 collected from both sampling lines, indicating that even submicron particles typical for the
278 AOS samples are of sea mist origin rather than sulfates formed by nucleation. Nucleated
279 sulfates presumably fall into the "S-rich" class and their relative population ranges from
280 between 2 – 6% and 15 – 30 % in the CVI and AOS samples, respectively. Relative
281 contributions of "other" particles normally remains at the 3 – 5% level and only occasionally
282 reaches values of 8 – 9%. Particle class composition remained largely the same over the
283 entire period of the cloudy episode for both sampling lines.

284 Figure 5 illustrates particle number size distributions of sea salt and S-rich particles
285 determined from the CCSEM/EDX data, combined for the 6 CVI and 6 AOS analyzed

286 samples. The four distributions are normalized to the total number of particles. Plots
287 presented in panels (a) and (b) are shown on the same scale to facilitate comparison. Hence,
288 areas below the distribution curves indicate relative populations of each particle class. The
289 size distributions in Figure 5 indicate a mode size of ~0.8 μm for residues of sea salt
290 particles in the CVI samples. A smaller mode size of 0.4-0.5 μm is observed for sea salt
291 particles in the AOS samples. The number concentration ratio of sea salt particles found in
292 the CVI samples to those in the AOS samples is approximately 2:1. The situation is reversed
293 for the S-rich particles where the concentration of S-rich particles in the AOS sample is ~2
294 times higher than for the CVI samples. The size distributions of S-rich particles peak at ~0.5
295 μm and ~0.4 μm for the CVI and AOS samples, respectively. However, the abrupt fall-off of
296 the size distributions at ~0.3-0.4 μm is due to the impactor cut-off function and
297 comparisons of the size distributions in Figure 5 must be made with this caveat in mind.

298 The CCSEM/EDX analysis indicates sulfur enrichment in sea salt particles. Figure 6
299 shows the CCSEM/EDX measured S/Na elemental ratios for sea salt particles detected in
300 the CVI (upper panel) and AOS (bottom panel) samples. The dashed horizontal line is the
301 nominal ratio of S/Na = 0.06, typical for sea water [*CRC*, 1999]. The solid curved line
302 indicates the experimentally determined deviation of the S/Na ratios for large sea salt
303 particles. This deviation is a result of ZAF sensitivity effects [*Goldstein, et al.*, 2003], which
304 were omitted from the quantification method [*Laskin and Cowin*, 2001; *Laskin, et al.*, 2006].
305 The S/Na elemental ratios are systematically higher than expected for unreacted sea salt
306 particles. This indicates cloud and chemical processing of sea salt particles with sulfur
307 compounds, which is consistent with the DMS chemistry expected in the region of this field
308 campaign.

309 For cloud and chemically processed sea salt particles, chemical reactions of sea salt
310 components and added sulfuric and/or methanesulfonic acids can be presented by the
311 following, highly simplified, albeit illustrative reactions:

312 $$2NaCl/MgCl_2(aq) + H_2SO_4(aq, g) \rightarrow Na_2SO_4/MgSO_4(aq) + 2HCl(g) \quad (1)$$

313 $$2NaCl/MgCl_2(aq) + CH_3SO_3H(aq, g) \rightarrow CH_3SO_3Na/(CH_3SO_3)_2Mg\,(aq) + 2HCl(g) \quad (2)$$

314 These reactions liberate HCl gas to the atmosphere, leaving particles enriched in sulfur and
315 depleted in chloride. Additional sulfur-halogen processes could also lead to similar changes
316 in the elemental composition of sea salt particles [*Finlayson-Pitts*, 2003; *Finlayson-Pitts and*
317 *Hemminger*, 2000]. However, a full discussion of the detailed reaction mechanism and its
318 kinetics is beyond the scope of this manuscript.

319 The sulfur enrichment is larger for sea salt particles in the CVI samples, compared to
320 those in the AOS samples. This is likely a result of the greater activation of particles (larger
321 droplets and higher water content) sampled in the CVI line, compared to the smaller sizes
322 sampled in the AOS line. If so, the higher water content would provide an enhanced
323 capacity for soluble species in larger droplets, and therefore higher S/Na ratios in the CVI
324 samples of dry residues would be expected.

325 CCSEM/EDX analysis provides quantitative data on the S/Na ratios over a
326 statistically significant number of particles. However, no molecular information on the
327 chemical forms of sulfur can be inferred from EDX spectroscopy. Molecular speciation of
328 sulfur-containing compounds is revealed by complementary analysis of individual particles
329 using TOF-SIMS. To identify chemical forms of sulfur, TOF-SIMS ionic maps were
330 produced for selected ions indicative of sulfate (SO_4^-, HSO_4^-), methanesulfonate (SO_3^-,
331 $CH_3SO_3^-$), sodium (Na^+) and ammonium (NH_4^+). Figure 7 shows ionic maps (100 μm × 100

μm) characteristic for CVI samples collected during this cloudy period. The maps indicate that methanesulfonate (SO_3^-, $CH_3SO_3^-$) ions are co-located with Na^+ ions, while sulfate (SO_4^{2-}, HSO_4^-) ions are co-located with NH_4^+ ions. Furthermore, the characteristic locations of sulfate and the methanesulfonate ions do not overlap. These observations support the conclusion that methanesulfonate is present in relatively large sea salt particles, while the characteristic sulfate ions are primarily generated from smaller $(NH_4)_2SO_4$ particles. To confirm this conclusion, TOF-SIMS negative spectra integrated from the areas of sea salt and $(NH_4)_2SO_4$ particles were compared with those acquired from laboratory prepared samples of CH_3SO_3Na and $(NH_4)_2SO_4$ particles. This comparison is shown in Figure 8. The characteristic spectra of field collected particles match those of the standard materials nearly perfectly. Although not shown here, negative spectra of Na_2SO_4, CH_3SO_4Na, and HO-CH_2SO_3Na particles were also measured (see supplement A), and did not match the spectra measured in the field samples.

However, these TOF-SIMS observations should be interpreted with some caution. Particles were examined with a low primary ion dose (static mode of operation), resulting in an analysis depth of 3 – 5 nm, thus corresponding to the outermost atomic layers of the particles. As particles dry out, the less soluble salts precipitate first and form the core of the particle, while more soluble salts are present in the outer layer. Thus, the observed abundant mass spectrometry signal originating from the highly soluble CH_3SO_3Na salt does not confirm the absence of sulfates in these sea salt particles as sulfates could be present at the particle core, and therefore not detectable in this operating mode of the TOF-SIMS instrument. Nevertheless, the important observation is that the $(NH_4)_2SO_4$ particles show little or no signal of $CH_3SO_3^-$ characteristic for methanesulfonate salts.

In principle, a combination of static and dynamic modes of operation of the TOF-SIMS allows monitoring of chemical speciation of compounds within particles [*Gaspar, et al.*, 2004; *Laskin, Gaspar, et al.*, 2003; *Liu, et al.*, 2007]. However, these experiments are technically challenging, and inherently qualitative, providing no quantitative information on the concentrations of different species within particles. An alternative approach uses STXM/NEXAFS analysis to study chemical bonding information of different elements for individual particles. Supported by the TOF-SIMS observations, this enables the speciation of different elements within particles allowing quantification of $CH_3SO_3^-/SO_4^{2-}$ ratios in individual particles.

Figure 9(a) shows a representative STXM image (12 μm × 12 μm) recorded at 290.8 eV of a sample region containing two particle classes observed in our experiments. Contours of the sea salt and the S-rich particles in the STXM image are marked by squares and circles, respectively. Maps generated by principle component analysis (PCA) of the acquired STXM/NEXAFS spectra are shown, with colors corresponding to X-ray absorbance regions specific for nitrogen, carbon and sulfur. In contrast to the TOF-SIMS maps, these PCA maps generated from STXM/NEXAFS analysis are indicative of the entire composition of sampled particles due to the fact that transmitted intensity through the sample is measured. Comparison of the PCA maps presented in Figure 9(b) and (c) shows that these particles either contain carbon or nitrogen, but not both elements. This observation is consistent with particles having either mixed sea salt/$CH_3SO_3^-/SO_4^{2-}$ (red) or mixed $H_2SO_4/(NH_4)_2SO_4$ (black) composition. The spectral contours of the N K-edge NEXAFS spectra of the mixed $H_2SO_4/(NH_4)_2SO_4$ and purchased $(NH_4)_2SO_4$ are nearly identical (unpublished data), which is further evidence that these small round particles are mixed $H_2SO_4/(NH_4)_2SO_4$. The low carbon absorption in purchased CH_3SO_3Na and the sea salt/$CH_3SO_3^-$/nss-SO_4^{2-} particles

made peak assignments in their spectra ambiguous, thus preventing comparisons of the C-K edge NEXAFS spectra. The PCA maps presented in Figure 9(d) indicate two different types of sulfur characteristic for two particle classes. The particles which contain nitrogen (black) display a sulfur L-edge NEXAFS spectrum indicative of SO_4^{2-} which is consistent with these particles being assigned as mixed $H_2SO_4/(NH_4)_2SO_4$. The particles which contain carbon (red) display a sulfur L-edge spectrum that is intermediate of $CH_3SO_3^-$ and SO_4^{2-}. This is consistent with these particles having a mixed sea salt/$CH_3SO_3^-$/SO_4^{2-} composition.

Furthermore, combined data sets from CCSEM/EDX and STXM/NEXAFS measurements, enable quantification of the $CH_3SO_3^-/SO_4^{2-}$ ratios on an individual particle basis. Elemental analysis performed using CCSEM/EDX measures the total S/Na ratio for a large number of particles. Separately, STXM/NEXAFS analysis provides quantification of the partitioning between $CH_3SO_3^-$ and total-SO_4^{2-} (nss and ss) on an individual particle basis. Combining these two data sets, in addition to the literature reported value for ss-SO_4^{2-}/Na = 0.06 [*CRC*, 1999], enables the total-SO_4^{2-} to be decoupled into nss and ss components, leading to the quantitative assessment of $CH_3SO_3^-$/nss-SO_4^{2-} ratios in particles as will be described below.

Figure 10(a) presents S L-edge NEXAFS spectra of the Na_2SO_4 and CH_3SO_3Na reference particles respectively. The Na_2SO_4 spectrum displays three distinct peaks at 170.9 eV, 172.1 eV and 172.9 eV, in good agreement with literature data [*Hitchcock, et al.*, 1990]. Sulfur spectra recorded from $(NH_4)_2SO_4$ and Na_2SO_4, both of which have an oxidation state of +6, were identical to one another. However, the CH_3SO_3Na spectrum is considerably different, its broad contour has no resolvable peaks and the peak maximum occurs at lower energy. The peak maximum of the Na_2SO_4 spectrum (or sulfate in general) appears at higher energy because of its higher oxidation state (+6 for Na_2SO_4 versus +5 for CH_3SO_3Na).

These differences in the spectral contours of SO_4^{2-} and CH_3SO^{3-} are advantageous for determining the partitioning between these two species in individual particles. Mixing of $CH_3SO_3^-$ and SO_4^{2-} in particle spectra would lead to a broadening of the resolved peaks present in SO_4^{2-} and a change in the relative intensities of the three peaks. These changes in spectral contours as a function of the proportion of $CH_3SO_3^-$ and SO_4^{2-} were used to quantify the amount of $CH_3SO_3^-$ and total-SO_4^{2-} present in individual particles. For example, the $CH_3SO_3^-$/total-SO_4^{2-} ratio from the single particle pertinent to Figure 10(b) is determined as 20:80%. The corresponding spectrum modeled for 20% $CH_3SO_3^-$ and 80% total-SO_4^{2-} is shown for comparison. A good agreement between the spectral contours is observed. Further details about the sulfur L-edge spectroscopy are provided in Supplement B.

As STXM/NEXAFS is significantly more time and labor intensive than CCSEM/EDX, a single CVI sample from the studied time period was selected for quantitative analysis. A CVI sample was chosen due to the higher proportion of mixed sea salt/$CH_3SO_3^-$/nss-SO_4^{2-} particles. Several other CVI and AOS samples from this time period were surveyed using STXM/NEXAFS, and confirmed qualitative observations reported for the selected sample in this publication. The STXM/NEXAFS analysis method was applied to sulfur L-edge spectra recorded from ~100 individual mixed sea salt/$CH_3SO_3^-$/nss-SO_4^{2-} particles to determine their $CH_3SO_3^-$/total-SO_4^{2-} ratio. In Figure 11 the $CH_3SO_3^-$/total-SO_4^{2-} ratio is plotted against the average particle diameter. As most particles are irregular in shape, the equivalent circle diameter was calculated from the particle projection area. The error bars displayed in Figure 11 represent the standard deviation in the mean $CH_3SO_3^-$/total-SO_4^{2-} ratio, which is derived from the calibration plot presented in Supplement B. No obvious size dependence was observed in the $CH_3SO_3^-$/total-SO_4^{2-} ratio

427 for the particles studied, which ranged from ~1 – 5 μm in diameter. Hence, the mean
428 $CH_3SO_3^-$/total-SO_4^{2-} ratio, represented by the solid black line in Figure 11 (the two dashed
429 lines are the standard deviation from the mean), yield a value of 0.52 with a standard
430 deviation of ± 0.30, assuming invariance with particle size.

431 Figure 12(a) presents the normalized distribution of the total-S/Na ratios detected in
432 over 7000 individual sea salt/$CH_3SO_3^-$/nss-SO_4^{2-} particles using the CCSEM/EDX
433 technique. The frequency of particles displaying a particular total S/Na ratio is normalized to
434 the total number of particles examined. This data is plotted for different size bins with
435 particle diameters ranging from 0.3 to > 2 μm. The size bins are set using the log(D_p) scale
436 with an even spacing of 0.2, where D_p represents particle diameter. The total S/Na ratio is
437 between 0.05 – 1 and peaks at 0.15 for particles in all size bins. This peak total S/Na value of
438 0.15 is higher than that characteristic for sea water (0.06) [*CRC*, 1999]. The higher observed
439 value can be understood by considering acid displacement reactions of $NaCl/MgCl_2$ present
440 in sea water with H_2SO_4 and CH_3SO_3H, which increase the total S present in the particles.
441 Sea salt fully reacted with H_2SO_4 would yield a total S/Na ratio of 0.59. Clearly, the range of
442 total S/Na values observed in these multi-component particles exceeds this, reaching values
443 as high as 1. Again, this higher observed value can be understood by considering reactions of
444 $NaCl/MgCl_2$ with CH_3SO_3H, which may yield a total S/Na ratio of 1.18. An enhancement in
445 the fraction of particles displaying total S/Na ratios > 0.15 is observed for smaller particles
446 that display larger surface-to-volume ratios. This observation could suggest that surface area
447 controls the uptake of gas-phase CH_3SO_3H by liquid sea salt particles. The longer average
448 atmospheric residence times of smaller particles may also increase the probability of reaction
449 resulting in $CH_3SO_3^-$ and nss-SO_4^{2-} enrichment.

As noted above, calculation of the $CH_3SO_3^-$/nss-SO_4^{2-} ratio relies on a combination of data recorded using both STXM/NEXAFS and CCSEM/EDX. The method for combining this data is presented here. For the mixed sea salt/$CH_3SO_3^-$/nss-SO_4^{2-} particles, the total S/Na ratio is equal to the sum of ss-SO_4^{2-}/Na, nss-SO_4^{2-}/Na and $CH_3SO_3^-$/Na ratios, as described by equation 3:

$$\frac{[\text{total-S}]}{[\text{Na}]} = \underbrace{\frac{[\text{ss-SO}_4^{2-}]}{[\text{Na}]}}_{=0.06} + \frac{[\text{nss-SO}_4^{2-}]}{[\text{Na}]} + \frac{[\text{CH}_3\text{SO}_3^-]}{[\text{Na}]} \quad (3)$$

The ss-SO_4^{2-}/Na ratio is 0.06 [*CRC*, 1999], leaving two unknowns in this equation. The $CH_3SO_3^-$/total-SO_4^{2-} ratio is determined as 0.52 ± 0.30 using the STXM/NEXAFS technique. This ratio can be written as follows:

$$\frac{[\text{CH}_3\text{SO}_3^-]}{[\text{total-SO}_4^{2-}]} = \frac{[\text{CH}_3\text{SO}_3^-]/[\text{Na}]}{[\text{total-SO}_4^{2-}]/[\text{Na}]} = \frac{[\text{CH}_3\text{SO}_3^-]/[\text{Na}]}{0.06 + [\text{nss-SO}_4^{2-}]/[\text{Na}]} \quad (4)$$

This leaves the same two unknowns as in equation 3. These two equations can now be solved to determine values for both [$CH_3SO_3^-$]/[Na] and [nss-SO_4^{2-}]/[Na].

This analysis method is applied to the data presented in Figure 12(a) to yield Figure 12(b), which displays the distribution of $CH_3SO_3^-$/nss-SO_4^{2-} in individual particles for different size bins. As particle diameter increases, the distribution of $CH_3SO_3^-$/nss-SO_4^{2-} shifts to higher values, *i.e.* sulfur in larger particles is mostly in the form of $CH_3SO_3^-$, while sulfur content in smaller particles is dominated by the SO_4^{2-} form.

The peak of the distribution presented in Figure 12(b), which uses the mean $CH_3SO_3^-$/total-SO_4^{2-} ratio of 0.52, yields a $CH_3SO_3^-$/nss-SO_4^{2-} partitioning ratio of 0.6. Using the standard deviation in the mean CH_3SO_3Na/total-SO_4^{2-} ratio of ±0.30, the lower and upper limits on the $CH_3SO_3^-$/nss-SO_4^{2-} ratio are calculated as 0.30 and 1.10. The large variation in this ratio could be attributed to differences in the individual particle history, the long duration over which the particles were sampled, the uncertainty associated with the measurement and the assumptions associated with invariance of $CH_3SO_3^-/SO_4^{2-}$ with particle size.

Therefore, all the observations presented in this manuscript so far, can be summarized as follows. Particles collected during the cloudy period between July 6th 17:00-July 7th 9:00 (PST) can be divided in two major particle classes: (a) sea salt particles composed of a mixture of sea salt/$CH_3SO_3^-/SO_4^{2-}$ and (b) S-rich particles of mixed $H_2SO_4/(NH_4)_2SO_4$ composition. Qualitatively, these observations are in agreement with the schematic of the sulfur-aerosol-climate links in the MBL in Figure 1. Indeed, the presence of $CH_3SO_3^-$ in sea salt particles indicates substantial formation and fast uptake of CH_3SO_3H by activated droplets containing sea salt presumably resulting from the oxygen addition channel in the DMS oxidation mechanism. Formation of mixed $H_2SO_4/(NH_4)_2SO_4$ particles is indicative of H_2SO_4 nucleation resulting from the H abstraction channel of DMS oxidation. Therefore, the quantitative assessment of partitioning between two different forms of sulfur, *i.e.* $CH_3SO_3^-$ and nss-SO_4^{2-}, is important for kinetic modeling as it is an inherent indicator of the pathways of DMS oxidation in the environment of the given geographic location. The partitioning between these reaction products is important for climate considerations as the result impacts the number and size of CCN produced in the marine atmosphere.

493 The $CH_3SO_3^-$/nss-SO_4^{2-}> 0.6 ratios in sea salt particles reported in this study are high
494 compared to previous measurements at similar latitudes. The reported ratios are similar to
495 those from polar latitudes where the temperature is lower, a factor known to enhance the
496 addition pathway leading to formation of $CH_3SO_3^-$. The results presented here are somewhat
497 comparable with model calculations which predict higher $CH_3SO_3^-$/nss-SO_4^{2-} ratios in the
498 summer for pristine marine air sampled under cold (276 K), cloudy conditions and implying
499 additional oxidation reactions of DMS with halogen radicals [*von Glasow and Crutzen*, 2004].
500 However, there is an important aspect of the presented data that contradicts modeling study
501 of *von Glasow and Crutzen* [2004]. The TOF-SIMS analysis of particle samples (see Fig. 7)
502 indicate that $CH_3SO_3^-$ is exclusively associated with sea salt particles, but not with
503 $(NH_4)_2SO_4$ particles. This finding disagrees with the modeling results that indicate significant
504 formation of $CH_3SO_3^-$ in sulfate particles as a result of their smaller size and higher surface-
505 to-volume ratio compared that typical for sea salt particles. Furthermore, despite their
506 different starting sizes, the sulfate and the sea salt particles would grow to aqueous droplets
507 that are roughly of the same size, if activated. As a result, the condensed compounds should
508 be quite similar in the different activated particles. This observed selectivity of $CH_3SO_3^-$ to
509 sea salt particles is quite puzzling and additional studies are required to understand this
510 discrepancy.

511 The discrepancy is even more intriguing given that our numerical model calculations
512 of the atmospheric chemistry occurring in the area of the field experiment suggests that
513 consideration of cloud chemistry is essentially required to explain the high $CH_3SO_3^-$/nss-
514 SO_4^{2-} and S/Na ratios reported in this study. These modeling results are presented and
515 discussed below.

516 During the cloudy period studied here, meteorological data indicate that air parcels
517 arriving to the sampling site were first swiftly transported from the open ocean area and then
518 turned southbound along the coastline of northern California (Figure 2) where it remained
519 for ~12-18 hours prior to sampling. A systematic analysis of phytoplankton pigment
520 concentrations in this area (derived from satellite based multi-annual records) indicate an
521 order of magnitude higher phytoplankton concentration in the narrow latitudinal range
522 adjacent to the shore. Specifically, within 100-200 km of the coast, typical concentrations of
523 phytoplankton of ~5 μg/l are reported, while 300-400 km offshore these decrease to ~0.5
524 μg/l [*A. C. Thomas and Strub*, 1990]. Therefore, the key factor determining the $CH_3SO_3^-$/nss-
525 SO_4^{2-} and total-S/Na ratios in sea salt particles is most likely the amount of time the air mass
526 spent in the area of high DMS emissions (high phytoplankton concentrations) which is in
527 the order of ~18 hours or less prior to sampling at Pt. Reyes.
528 A Lagrangian box-model [*Zaveri*, 1997] was used to simulate atmospheric oxidation
529 of DMS in the air mass that originated over unpolluted open ocean areas and entered the
530 region of high DMS concentration ~18 hour prior to the sampling which corresponds to ~
531 6 am local time. Two model scenarios were examined: (a) gas-phase chemistry only, and (b)
532 coupled gas- and cloud-phase chemistry. The initial conditions for model runs and a brief
533 description of the model are given in supplement C.
534 Figure 13 shows the temporal evolution of DMS, $CH_3SO_3^-$/nss-SO_4^{2-}, and total
535 S/Na for gas-chemistry only and coupled gas- and cloud-phase chemistry scenarios. A few
536 hours are required to build up the SO_2 concentration from gas-phase DMS oxidation in the
537 relatively clean air mass as it was advected along the coast over high DMS emissions region
538 for the next 12-18 hours. During this time, $CH_3SO_3^-$ is efficiently formed in particles, while
539 formation of nss-SO_4^{2-} is somewhat delayed. The gas-chemistry-only model results indicate

that the $CH_3SO_3^-$/nss-SO_4^{2-} ratio in sea salt particles reaches a maximum of ~0.18 during the early stages of DMS oxidation (<6 hours) because formation of CH_3SO_3H proceeds more rapidly early in the day when compared to H_2SO_4 formation. Later, as both OH and SO_2 concentrations increase, formation of H_2SO_4 begins to exceed that of CH_3SO_3H, resulting in a decrease in the particulate $CH_3SO_3^-$/nss-SO_4^{2-} ratio to a quasi-steady-state value of ~0.13, which is about a factor of 5 lower than the observed ratios seen in Figure 11b. Also, a negligible increase in the modeled values of the total-S/Na ratio is seen even after 18 hours of processing, which is at odds with the measurements for the field-collected sea salt particles as seen in Figure 11a.

Atmospheric conditions during our field study most likely resemble the coupled gas and cloud chemistry scenario. Indeed, the coupled gas- and cloud-phase model results show that the $CH_3SO_3^-$/nss-SO_4^{2-} bulk ratio in sea salt particles reached a maximum of ~0.3 in ~6 hours and then remained fairly steady for the rest of the simulation period. This value is comparable within a factor of ~2 to our measurements. Also, the total-S/Na bulk ratio is predicted to increase up to ~0.09 in 12 hours, which is similar to the observed values. These results therefore suggest that cloud-phase oxidation of SO_2, DMS, DMSO, MSIA, and MSA played an important role under the atmospheric conditions encountered during this field study.

We note that the purpose of these modeling calculations is to evaluate the feasibility of the plausible hypothesis rather than providing detailed cross-comparison between field and modeling data, which lies beyond the scope of this manuscript. With this regard, it is important to note that modeled $CH_3SO_3^-$/nss-SO_4^{2-} and total-S/Na ratios is sensitive to a number of parameters, which include DMS flux, temperature, sea-salt particle concentration and size distribution, and photolysis rate. Additionally, halogen chemistry and nucleation

564 (new particle formation) were neglected in the present model, but may play an important
565 role. The influence of these parameters are interesting topics for more detailed modeling
566 studies where the field data provided here could be used for validation.
567
568 **5. CONCLUSIONS AND ATMOPHERIC IMPLICATIONS**
569 This study presents the first observations of both $CH_3SO_3^-$ and SO_4^{2-} sulfur
570 compounds in marine aerosol, identified on a single particle basis. Both TOF-SIMS and
571 STXM/NEXAFS techniques indicate an external mixture consisting primarily of two
572 particle classes; mixed sea salt/$CH_3SO_3^-$/SO_4^{2-} and S-rich particles of mixed
573 H_2SO_4/$(NH_4)_2SO_4$ composition. Unambiguous, qualitative speciation of sulfur containing
574 compounds and quantitative assessment of the $CH_3SO_3^-$/nss-SO_4^{2-} ratios are facilitated
575 using combined data sets from three techniques: CCSEM/EDX – quantitative assessment of
576 elemental composition of individual particles, TOF-SIMS – qualitative molecular speciation
577 of sulfur-containing compounds in individual particles, STXM/NEXAFS – quantitative
578 assessment of different forms of sulfur within individual particles. The data provided by
579 these techniques offer a rich set of qualitative and quantitative information that is of primary
580 importance to atmospheric processes in the MBL involving sea salt and marine sulfate
581 particles.

582 For the first time, size-dependent nss-S/Na and $CH_3SO_3^-$/nss-SO_4^{2-} ratios are
583 reported for marine particles. Characteristic ratios of nss-S/Na > 0.10 are reported for sea
584 salt particles, with higher values observed for smaller particles, indicating more extensive
585 formation of sulfur-containing salts. Characteristic ratios of $CH_3SO_3^-$/nss-SO_4^{2-} > 0.60 are
586 reported for sea salt particles of all sizes, with higher values for large particles. This indicates

587 that $CH_3SO_3^-$ salts are likely the dominant form of nss-sulfur in large particles while SO_4^{2-} is
588 more common in smaller particles.

589 In the past, much attention has been given to the hygroscopic and optical properties
590 of sea salt aerosol and the corresponding mixed sea salt/sulfate particles that can be formed
591 as a result of the DMS→SO_2→H_2SO_4 reaction sequence that is assumed to dominate in the
592 mid-latitude marine boundary layer. However, our analysis of field collected sea salt particles
593 and presented in this manuscript indicate that DMS conversion to MSA can result in
594 $CH_3SO_3^-/SO_4^{2-}$ >0.6 and nss-S/Na >0.1 ratios, as were observed under specific conditions
595 of the coastal area north of San Francisco. These findings indicate that modeling of the
596 marine boundary layer (MBL) aerosols and cloud formation processes require extensive data
597 on the hygroscopic and CCN properties of mixed sea salt/$CH_3SO_3^-/SO_4^{2-}$ and perhaps other
598 organo-sulfur particles. These data are fairly scarce and require future research.

599

Acknowledgments

The authors gratefully acknowledge E. Andrews, J.A. Ogren, B.T. Jobson, M.L. Alexander and N.S. Laulainen for arranging and the cooperation at the Point Reyes sampling site, D. J. Gaspar for providing important guidance and access to the TOF-SIMS instrument, and A. L. D. Kilcoyne - scientist at beamline 5.3.2. The help of M. Khaiyer of NASA Cloud and Radiation group at NASA Langley Research Center is greatly acknowledged for the retrieval of the satellite image. R.J. Hopkins acknowledges sponsorship provided by the 2006 Summer Research Institute on Interfacial and Condensed Phase Chemical Physics organized at PNNL. Financial support for this study was provided by the Atmospheric Science Program of the Department of Energy's office of Biological and Environmental Research. The CCSEM/EDX and TOF-SIMS particle analyses were performed in the Environmental Molecular Sciences Laboratory, a national scientific user facility sponsored by the Department of Energy's Office of Biological and Environmental Research at Pacific Northwest National Laboratory. PNNL is operated by the U.S. Department of Energy by Battelle Memorial Institute under contract DE-AC06-76RL0. The work at the ALS was partially supported by the Director, Office of Science, Office of Basic Energy Sciences, Division of Chemical Sciences, Geosciences, and Biosciences of the U.S. Department of Energy at Lawrence Berkeley National Laboratory under Contract No. DE-AC02-05CH11231.

Supplemental Information Available:

Supplement A - TOF-SIMS spectra of particles prepared from purchased standard materials.

Supplement B - Determination of $CH_3SO_3^-$/total-SO_4^{2-} ratio in individual sea salt particles

Supplement C - Description of the model and key constraints.

623 **References**

624 Allen, A. G., A. L. Dick, and B. M. Davison (1997), Sources of atmospheric
625 methanesulphonate, non-sea-salt sulphate, nitrate and related species over the
626 temperate South Pacific, *Atmospheric Environment*, *31*, 191-205.

627 Andreae, M. O., and H. Raemdonck (1983), Dimethyl Sulfide in the Surface Ocean and the
628 Marine Atmosphere - a Global View, *Science*, *221*, 744-747.

629 Andreae, T. W., M. O. Andreae, H. G. Bingemer, and C. Leck (1993), Measurements of
630 Dimethyl Sulfide and H_2S over the Western North-Atlantic and the Tropical
631 Atlantic, *Journal of Geophysical Research-Atmospheres*, *98*, 23389-23396.

632 Arsene, C., I. Barnes, K. H. Becker, W. F. Schneider, T. T. Wallington, N. Mihalopoulos,
633 and I. V. Patroescu-Klotz (2002), Formation of methane sulfinic acid in the gas-
634 phase OH-radical initiated oxidation of dimethyl sulfoxide, *Environmental Science and*
635 *Technology*, *36*, 5155-5163.

636 Bandy, A. R., D. L. Scott, B. W. Blomquist, S. M. Chen, and D. C. Thornton (1992), Low
637 Yields of SO_2 from Dimethyl Sulfide Oxidation in the Marine Boundary-Layer,
638 *Geophysical Research Letters*, *19*, 1125-1127.

639 Bandy, A. R., D. C. Thornton, F. H. Tu, B. W. Blomquist, W. Nadler, G. M. Mitchell, and
640 D. H. Lenschow (2002), Determination of the vertical flux of dimethyl sulfide by
641 eddy correlation and atmospheric pressure ionization mass spectrometry (APIMS),
642 *Journal of Geophysical Research-Atmospheres*, *107 (D24),* Art. No. 4743,
643 doi:10.1029/2002JD002472

644 Bardouki, H., M. B. da Rosa, N. Mihalopoulos, W.U. Palm, C. Zetzsch. (2002), Kinetics and
645 Mechanism of the Oxidation of Dimethylsulfoxide (DMSO) and Methanesulfinate
646 (MSI^-) by OH Radicals in Aqueous Medium, *Atmos. Environ., 36,* 4627–4634.

647 Barnard, W. R., M. O. Andreae, W. E. Watkins, H. Bingemer, and H. W. Georgii (1982), The
648 Flux of Dimethylsulfide from the Oceans to the Atmosphere, *Journal of Geophysical*
649 *Research-Oceans and Atmospheres*, *87*, 8787-8793.

650 Barnes, I., K. H. Becker, and N. Mihalopoulos (1994), An FTIR Product Study of the
651 Photooxidation of Dimethyl Disulfide, *Journal of Atmospheric Chemistry*, *18*, 267-289.

652 Bates, T. S., B. K. Lamb, A. Guenther, J. Dignon, and R. E. Stoiber (1992), Sulfur Emissions
653 to the Atmosphere from Natural Sources, *Journal of Atmospheric Chemistry*, *14*, 315-337.

654 Barone, S. B., A. A.Turnipseed, A. R. Ravishankara (1996), Reaction of OH with dimethyl
655 sulfide (DMS). 1. Equilibrium constant for OH+DMS reaction and the kinetics of
656 the OH•DMS+O_2 reaction, *J. Phys. Chem., 100 (35),* 14694-14702.

657 Berresheim, H., M. O. Andreae, G. P. Ayers, R. W. Gillett, J. T. Merrill, V. J. Davis, and W.
658 L. Chameides (1990), Airborne Measurements of Dimethylsulfide, Sulfur-Dioxide,
659 and Aerosol Ions over the Southern-Ocean South of Australia, *Journal of Atmospheric*
660 *Chemistry*, *10*, 341-370.

661 Burgermeister, S., and H. W. Georgii (1991), Distribution of Methanesulfonate, nss-Sulfate
662 and Dimethylsulfide over the Atlantic and the North-Sea, *Atmospheric Environment*
663 *Part a-General Topics*, *25*, 587-595.

664 Charlson, R. J., J. E. Lovelock, M. O. Andreae, and S. G. Warren (1987), Oceanic
665 Phytoplankton, Atmospheric Sulfur, Cloud Albedo and Climate, *Nature*, *326*, 655-
666 661.

667 Cooper, D. J., and E. S. Saltzman (1991), Measurements of Atmospheric Dimethyl Sulfide
668 and Carbon-Disulfide in the Western Atlantic Boundary-Layer, *Journal of Atmospheric*
669 *Chemistry*, *12*, 153-168.

670 Cooper, D. J., and E. S. Saltzman (1993), Measurements of Atmospheric Dimethylsulfide,
671 Hydrogen-Sulfide, and Carbon-Disulfide During Gte Cite-3, *Journal of Geophysical*
672 *Research-Atmospheres*, *98*, 23397-23409.

673 Covert, D. S., V. N. Kapustin, P. K. Quinn, and T. S. Bates (1992), New Particle Formation
674 in the Marine Boundary-Layer, *Journal of Geophysical Research-Atmospheres*, *97*, 20581-
675 20589.

676 CRC (1999), Handbook of Chemistry and Physics. A ready-reference book of chemical and
677 physics data., 80th, ed., D. R. Lide, CRC Press Inc., Boca Raton, FL.

678 Draxler, R. R., and G. D. Rolph (2003), HYSPLIT (HYbrid Single-Particle Lagrangian
679 Integrated Trajectory) Model access via NOAA ARL READY Website
680 (http://www.arl.noaa.gov/ready/hysplit4.html). NOAA Air Resources Laboratory,
681 Silver Spring, MD.

682 Finlayson-Pitts, B. J. (2003), The tropospheric chemistry of sea salt: A molecular-level view
683 of the chemistry of NaCl and NaBr, *Chemical Reviews*, *103*, 4801-4822.

684 Finlayson-Pitts, B. J., and J. C. Hemminger (2000), Physical chemistry of airborne sea salt
685 particles and their components, *Journal of Physical Chemistry A*, *104*, 11463-11477.

686 Galloway, J. N., D. L. Savoie, W. C. Keene, and J. M. Prospero (1993), The Temporal and
687 Spatial Variability of Scavenging Ratios for nss-Sulfate, Nitrate, Methanesulfonate
688 and Sodium in the Atmosphere over the North-Atlantic Ocean, *Atmospheric*
689 *Environment Part a-General Topics*, *27*, 235-250.

690 Ganor, E., H. A. Foner, H. G. Bingemer, R. Udisti, and I. Setter (2000), Biogenic sulphate
691 generation in the Mediterranean Sea and its contribution to the sulphate anomaly in
692 the aerosol over Israel and the Eastern Mediterranean, *Atmospheric Environment*, *34*,
693 3453-3462.

694 Gaspar, D. J., A. Laskin, W. Wang, S. W. Hunt, and B. J. Finlayson-Pitts (2004), TOF-SIMS
695 analysis of sea salt particles: imaging and depth profiling in the discovery of an
696 unrecognized mechanism for pH buffering, *Applied Surface Science*, *231-2*, 520-523.

697 Goldstein, J. I., D. E. Newbury, P. Echlin, D. C. Joy, C. E. Lyman, E. Lifshin, L. Sawyer,
698 and J. R. Michael (2003), *Scanning Electron Microscopy and X-ray Microanalysis*, Third
699 Edition ed., Kluwer, New York.

700 Gong, S. L. (2003), A parameterization of sea-salt aerosol source function for sub- and
701 super-micron particles, *Global Biogeochemical Cycles*, *17(4)*, Art. No. 1097,
702 doi:10.1029/2003GB002079.

703 Gong, S. L., and L. A. Barrie (2003), Simulating the impact of sea salt on global nss sulphate
704 aerosols, *Journal of Geophysical Research-Atmospheres*, *108 (D16)*, Art. No. 4516,
705 doi:10.1029/2002JD003181.

706 Gong, S. L., L. A. Barrie, and J. P. Blanchet (1997), Modeling sea-salt aerosols in the
707 atmosphere.1. Model development, *Journal of Geophysical Research-Atmospheres*, *102*,
708 3805-3818.

709 Gong, S. L., L. A. Barrie, and M. Lazare (2002), Canadian Aerosol Module (CAM): A size-
710 segregated simulation of atmospheric aerosol processes for climate and air quality
711 models - 2. Global sea-salt aerosol and its budgets, *Journal of Geophysical Research-*
712 *Atmospheres*, *107 (D24),* Art. No. 4779, doi:10.1029/2001JD002004.

713 Hertel, O., J. Christensen, and O. Hov (1994), Modeling of the End-Products of the
714 Chemical Decomposition of DMS in the Marine Boundary-Layer, *Atmospheric*
715 *Environment*, *28*, 2431-2449.

716 Hitchcock, A. P., G. Tourillon, R. Garrett, G. P. Williams, C. Mahatsekake, and C. Andrieu
717 (1990), Inner-shell excitation of gas-phase and polymer thin-film 3-alkylthiophenes
718 by electron energy loss and X-ray photoabsorption spectroscopy, *Journal of Physical*
719 *Chemistry*, *94*, 2327-2333.

720 Hopkins, R. J., A. V. Tivanski, B. D. Marten, and M. K. Gilles (2007), Chemical bonding and
721 structural information of black carbon reference materials and individual
722 carbonaceous atmospheric aerosols, *Journal of Aerosol Science*, *38*, 573-591.

723 Hynes, A. J., R. B. Stoker, A. J. Pounds, T. McKay, J. D. Bradshaw, J. M. Nicovich, and P.
724 H. Wine (1995), A Mechanistic Study of the Reaction of OH with Dimethyl-D(6)
725 Sulfide - Direct Observation of Adduct Formation and the Kinetics of the Adduct
726 Reaction with O_2, *Journal of Physical Chemistry*, *99*, 16967-16975.

727 Hynes, A. J., and P. H. Wine (1996), The atmospheric chemistry of dimethylsulfoxide
728 (DMSO) and mechanism of the OH+DMSO reaction, *Journal of Atmospheric*
729 *Chemistry*, *24*, 23-37.

730 Hynes, A. J., P. H. Wine, and D. H. Semmes (1986), Kinetics and Mechanism of OH
731 Reactions with Organic Sulfides, *Journal of Physical Chemistry*, *90*, 4148-4156.

732 Keller, M., W. Bellows, and R. Guillard (1989), Dimethylsulfide Production in Marine
733 Phytoplankton in *Biogenic Sulfur in the Environment*, edited by E. Saltzman and W.
734 Cooper, pp. 167-182, ACS, Washington, DC.

735 Kerminen, V. M., R. E. Hillamo, and A. S. Wexler (1998), Model simulations on the
736 variability of particulate MSA to non-sea-salt sulfate ratio in the marine environment,
737 *Journal of Atmospheric Chemistry*, *30*, 345-370.

738 Kettle, A.J., M.O. Andreae, D. Amouroux, T.W. Andreae, T.S. Bates, H. Berresheim, H.
739 Bingemer, R. Boniforti, M.A.J. Curran, G.R. Di Tullio, G. Helas, G.B. Jones, M.D.
740 Keller, R.P. Kiene, C. Leck, M. Levasseur, G. Malin, M. Maspero, P. Matrai, A.R.
741 McTaggart, N. Mihalopoulos, B.C. Nguyen, A. Novo, J.P. Putaud, S. Rapsomanikis,
742 G. Roberts, G. Schebeske, S. Sharma, R. Simo, R. Staubes, S. Turner and G. Uher
743 (1999), A global database of sea surface dimethylsulfide (DMS) measurements and a
744 procedure to predict sea surface DMS as a function of latitude, longitude and month,
745 *Global Biogeochem. Cycles, 13,* 399–444.

746 Kloster, S., J. Feichter, E. M. Reimer, K. D. Six, P. Stier, and P. Wetzel (2006), DMS cycle in
747 the marine ocean-atmosphere system - a global model study, *Biogeosciences*, *3*, 29-51.

748 Koga, S., and H. Tanaka (1993), Numerical Study of the Oxidation Process of
749 Dimethylsulfide in the Marine Atmosphere, *Journal of Atmospheric Chemistry*, *17*, 201-
750 228.

751 Koga, S., and H. Tanaka (1996), Simulations of seasonal variations of sulfur compounds in
752 the remote marine atmosphere, *Journal of Atmospheric Chemistry*, *23*, 163-192.

753 Koga, S., and H. Tanaka (1999), Modeling the methanesulfonate to non-sea-salt sulfate
754 molar ratio and dimethylsulfide oxidation in the atmosphere, *Journal of Geophysical*
755 *Research-Atmospheres*, *104*, 13735-13747.

756 Koga, S., H. Tanaka, M. Yamato, T. Yamanouchi, F. Nishio, and Y. Iwasaka (1991),
757 Methanesulfonic-Acid and Non-Sea-Salt Sulfate over Both Hemispheric Oceans,
758 *Journal of the Meteorological Society of Japan*, *69*, 1-14.

759 Kouvarakis, G., and N. Mihalopoulos (2002), Seasonal variation of dimethylsulfide in the gas
760 phase and of methanesulfonate and non-sea-salt sulfate in the aerosols phase in the
761 Eastern Mediterranean atmosphere, *Atmospheric Environment*, *36*, 929-938.

762 Laskin, A., and J. P. Cowin (2001), Automated single particle SEM/EDX analysis of
763 submicrometer particles down to 0.1 mu m, *Analytical Chemistry*, *73*, 1023-1029.

764 Laskin, A., J. P. Cowin, and M. J. Iedema (2006), Analysis of individual environmental
765 particles using modern methods of electron microscopy and X-ray microanalysis,
766 *Journal of Electron Spectroscopy and Related Phenomena*, *150*, 260-274.

767 Laskin, A., D. J. Gaspar, W. H. Wang, S. W. Hunt, J. P. Cowin, S. D. Colson, and B. J.
768 Finlayson-Pitts (2003), Reactions at interfaces as a source of sulfate formation in sea-
769 salt particles, *Science*, *301*, 340-344.

770 Laskin, A., M. J. Iedema, and J. P. Cowin (2003), Time-resolved aerosol collector for
771 CCSEM/EDX single-particle analysis, *Aerosol Science and Technology*, *37*, 246-260.

772 Lewis, E. R., and S. E. Schwartz (2004), *Sea Salt Aerosol Production: Mechanisms, Methods,*
773 *Measurements and Models - A Critical Review*, 413 pp., AGU, Washington, DC.

774 Li, S. M., and L. A. Barrie (1993), Biogenic Sulfur Aerosol in the Arctic Troposphere.1.
775 Contributions to Total Sulfate, *Journal of Geophysical Research-Atmospheres*, *98*, 20613-
776 20622.

777 Li, S. M., L. A. Barrie, and A. Sirois (1993), Biogenic Sulfur Aerosol in the Arctic
778 Troposphere.2. Trends and Seasonal-Variations, *Journal of Geophysical Research-*
779 *Atmospheres*, *98*, 20623-20631.

780 Li, S. M., L. A. Barrie, R. W. Talbot, R. C. Harriss, C. I. Davidson, and J. L. Jaffrezo (1993),
781 Seasonal and Geographic Variations of Methanesulfonic-Acid in the Arctic
782 Troposphere, *Atmospheric Environment Part a-General Topics*, *27*, 3011-3024.

783 Li, S. M., L. A. Barrie, and D. Toom (1996), Seasonal variations of methanesulfonate, non-
784 sea-salt sulfate, and sulfur dioxide at three sites in Canada, *Journal of Geophysical*
785 *Research-Atmospheres*, *101*, 4165-4173.

786 Liss, P. S., and L. Merlivat (1986), Air-sea gass exchange rates, in *The Role of Air-Sea Exchange*
787 *in Geochemical Cycling*, edited by P. Buat-Menard, pp. 113-127, Reidel, Dordrecht.

788 Liu, Y., Z. Yang, Y. Desyaterik, P. L. Gassman, H. Wang, and A. Laskin (2007), Probing
789 Hygroscopic Properties of Atmospheric Particles Using Complementary Methods of
790 Micro FTIR Spectroscopy and Micro Analyses, *Environmental Science and Technology*,
791 submitted.

792 Lucas, D. D., and R. G. Prinn (2002), Mechanistic studies of dimethylsulfide oxidation
793 products using an observationally constrained model, *Journal of Geophysical Research-*
794 *Atmospheres*, *107(D14),* Art. No. 4201, doi:10.1029/2001JD000843.

795 Lucas, D. D., and R. G. Prinn (2003), Tropospheric distributions of sulfuric acid-water
796 vapor aerosol nucleation rates from dimethylsulfide oxidation, *Geophysical Research*
797 *Letters*, *30 (22),* Art. No. 2136, doi:10.1029/2003GL018370.

798 Lucas, D. D., and R. G. Prinn (2005a), Parametric sensitivity and uncertainty analysis of
799 dimethylsulfide oxidation in the clear-sky remote marine boundary layer, *Atmospheric*
800 *Chemistry and Physics*, *5*, 1505-1525.

801 Lucas, D. D., and R. G. Prinn (2005b), Sensitivities of gas-phase dimethylsulfide oxidation
802 products to the assumed mechanisms in a chemical transport model, *Journal of*
803 *Geophysical Research-Atmospheres*, *110*, Art. No. D21312, doi:10.1029/2004JD005386

804 Maria, S. F., L. M. Russell, M. K. Gilles, and S. C. B. Myneni (2004), Organic aerosol growth
805 mechanisms and their climate-forcing implications, *Science*, *306*, 1921-1924.

806 MASE (2005), Marine Stratus Experiment (MASE) 2005, URL:
807 http://www.asp.bnl.gov/MASE.html.

808 Mihalopoulos, N., B. C. Nguyen, C. Boissard, J. M. Campin, J. P. Putaud, S. Belviso, I.
809 Barnes, and K. H. Becker (1992), Field-Study of Dimethylsulfide Oxidation in the
810 Boundary-Layer - Variations of Dimethylsulfide, Methanesulfonic-Acid, Sulfur-
811 Dioxide, Non-Seasalt Sulfate and Aitken Nuclei at a Coastal Site, *Journal of*
812 *Atmospheric Chemistry*, *14*, 459-477.

813 Murphy, D. M., J. R. Anderson, P. K. Quinn, L. M. McInnes, F. J. Brechtel, S. M.
814 Kreidenweis, A. M. Middlebrook, M. Posfai, D. S. Thomson, and P. R. Buseck
815 (1998), Influence of sea-salt on aerosol radiative properties in the Southern Ocean
816 marine boundary layer, *Nature*, *392*, 62-65.

817 Ogren, J. A., J. Heintzenberg, and R. J. Charlson (1985), In-situ Sampling of Clouds with a
818 Droplet to Aerosol Converter, *Geophysical Research Letters*, *12*, 121-124.

819 Quinn, P. K., D. S. Covert, T. S. Bates, V. N. Kapustin, D. C. Ramseybell, and L. M.
820 McInnes (1993), Dimethylsulfide Cloud Condensation Nuclei Climate System -
821 Relevant Size-Resolved Measurements of the Chemical and Physical-Properties of
822 Atmospheric Aerosol-Particles, *Journal of Geophysical Research-Atmospheres*, *98*, 10411-
823 10427.

824 Ravishankara, A.R., Y. Rudich, R. Talukdar, S.B. Barone, (1997) Oxidation of atmospheric
825 reduced sulphur compounds: Perspective from laboratory studies, *Philosophical Trans.*
826 *Royal Soc. London. Series B -Biological Sci, 352 (1350)*, 171-181.

827 Russell, L. M., S. F. Maria, and S. C. B. Myneni (2002), Mapping organic coatings on
828 atmospheric particles, *Geophysical Research Letters*, *29*, 1779.

829 Saltzman, E. S., D. L. Savoie, J. M. Prospero, and R. G. Zika (1985), Atmospheric
830 Methanesulfonic-Acid and Non-Sea-Salt Sulfate at Fanning and American Samoa,
831 *Geophysical Research Letters*, *12*, 437-440.

832 Saltzman, E. S., D. L. Savoie, J. M. Prospero, and R. G. Zika (1986), Methanesulfonic-Acid
833 and Non-Sea-Salt Sulfate in Pacific Air - Regional and Seasonal-Variations, *Journal of*
834 *Atmospheric Chemistry*, *4*, 227-240.

835 Saltzman, E. S., D. L. Savoie, R. G. Zika, and J. M. Prospero (1983), Methane Sulfonic-Acid
836 in the Marine Atmosphere, *Journal of Geophysical Research-Oceans and Atmospheres*, *88*,
837 897-902.

838 Sciare, J., E. Baboukas, M. Kanakidou, U. Krischke, S. Belviso, H. Bardouki, and N.
839 Mihalopoulos (2000), Spatial and temporal variability of atmospheric sulfur-
840 containing gases and particles during the Albatross campaign, *Journal of Geophysical*
841 *Research-Atmospheres*, *105*, 14433-14448.

842 Shaw, G. E. (1983), Bio-Controlled Thermostasis Involving the Sulfur Cycle, *Climatic Change*,
843 *5*, 297-303.

844 Sievering, H., J. Boatman, J. Galloway, W. Keene, Y. Kim, M. Luria, and J. Ray (1991),
845 Heterogeneous Sulfur Conversion in Sea-Salt Aerosol-Particles - the Role of Aerosol
846 Water-Content and Size Distribution, *Atmospheric Environment Part a-General Topics*, *25*,
847 1479-1487.

848 Sievering, H., J. Cainey, M. Harvey, J. McGregor, S. Nichol, and P. Quinn (2004), Aerosol
849 non-sea-salt sulfate in the remote marine boundary layer under clear-sky and normal
850 cloudiness conditions: Ocean-derived biogenic alkalinity enhances sea-salt sulfate
851 production by ozone oxidation, *Journal of Geophysical Research-Atmospheres*, *109,* Art.
852 No. D19317, doi:10.1029/2003JD004315.

853 Spicer, C. W., D. V. Kenny, E. Chapman, K. M. Busness, and C. M. Berkowitz (1996),
854 Observations of dimethyl sulfide over the western North Atlantic Ocean using an
855 airborne tandem mass spectrometer, *Journal of Geophysical Research-Atmospheres*, *101*,
856 29137-29147.

857 Spiro, P. A., D. J. Jacob, and J. A. Logan (1992), Global Inventory of Sulfur Emissions with
858 1' × 1' Resolution, *Journal of Geophysical Research-Atmospheres*, *97*, 6023-6036.

859 Stickel, R. E., J. M. Nicovich, S. Wang, Z. Zhao, and P. H. Wine (1992), Kinetic and
860 Mechanistic Study of the Reaction of Atomic Chlorine with Dimethyl Sulfide, *Journal*
861 *of Physical Chemistry*, *96*, 9875-9883.

862 Strub, P. T., C. James, A. C. Thomas, and M. R. Abbott (1990), Seasonal and Nonseasonal
863 Variability of Satellite-Derived Surface Pigment Concentration in the California
864 Current, *Journal of Geophysical Research-Oceans*, *95*, 11501-11530.

865 Thomas, A., and P. T. Strub (2001), Cross-shelf phytoplankton pigment variability in the
866 California Current, *Continental Shelf Research*, *21*, 1157-1190.

867 Thomas, A. C., and P. T. Strub (1990), Seasonal and Interannual Variability of Pigment
868 Concentrations across a California Current Frontal Zone, *Journal of Geophysical*
869 *Research-Oceans*, *95*, 13023-13042.

870 Thompson, A. M., and O. C. Zafiriou (1983), Air-sea fluxes of transient atmospheric species,
871 *Journal of Geophysical Research - Atmospheres*, *88*, 6696-6708.

872 Tivanski, A. V., R. J. Hopkins, T. Tyliszczak, and M. K. Gilles (2007), Oxygenated interface
873 on biomass burn tar balls determined by single particle scanning transmission X-ray
874 microscopy, *Journal of Physical Chemistry A*, *111*, 5448-5458.

875 Turnipseed, A. A., S. B. Barone, A. R. Ravishankara (1996), Reaction of OH with dimethyl
876 sulfide .2. Products and mechanisms, *J. Phys. Chem., 100(35),* 14703-14713

877 Urbanski, S. P., R. E. Stickel, and P. H. Wine (1998), Mechanistic and kinetic study of the
878 gas-phase reaction of hydroxyl radical with dimethyl sulfoxide, *Journal of Physical*
879 *Chemistry A*, *102*, 10522-10529.

880 von Glasow, R., and P. J. Crutzen (2004), Model study of multiphase DMS oxidation with a
881 focus on halogens, *Atmospheric Chemistry and Physics*, *4*, 589-608.

882 von Glasow, R., R. Sander, A. Bott, and P. J. Crutzen (2002a), Modeling halogen chemistry
883 in the marine boundary layer - 1. Cloud-free MBL, *Journal of Geophysical Research-*
884 *Atmospheres*, *107 (D17)*, Art. No. 4341, doi:10.1029/2001JD000942

885 von Glasow, R., R. Sander, A. Bott, and P. J. Crutzen (2002b), Modeling halogen chemistry
886 in the marine boundary layer - 2. Interactions with sulfur and the cloud-covered
887 MBL, *Journal of Geophysical Research-Atmospheres*, *107 (D17),* Art. No. 4323,
888 doi:10.1029/2001JD000943.

889 Wong, C. S., S. E. Wong, W. A. Richardson, G. E. Smith, M. D. Arychuk, and J. S. Page
890 (2005), Temporal and spatial distribution of dimethylsulfide in the subarctic
891 northeast Pacific Ocean: a high-nutrient-low-chlorophyll region, *Tellus Series B-*
892 *Chemical and Physical Meteorology*, *57*, 317-331.

893 Wylie, D. J., and S. J. deMora (1996), Atmospheric dimethylsulfide and sulfur species in
894 aerosol and rainwater at a coastal site in New Zealand, *Journal of Geophysical Research-*
895 *Atmospheres*, *101*, 21041-21049.

896 Yin, F. D., D. Grosjean, R. C. Flagan, and J. H. Seinfeld (1990), Photooxidation of Dimethyl
897 Sulfide and Dimethyl Disulfide. 2. Mechanism Evaluation, *Journal of Atmospheric*
898 *Chemistry*, *11*, 365-399.

899 Yin, F. D., D. Grosjean, and J. H. Seinfeld (1986), Analysis of Atmospheric Photooxidation
900 Mechanisms for Organosulfur Compounds, *Journal of Geophysical Research-Atmospheres*,
901 *91*, 14417-14438.

902 Yin, F. D., D. Grosjean, and J. H. Seinfeld (1990), Photooxidation of Dimethyl Sulfide and
903 Dimethyl Disulfide. 1. Mechanism Development, *Journal of Atmospheric Chemistry*, *11*,
904 309-364.

905 Zaveri, R. A. (1997), Development and Evaluation of a Comprehensive Tropospheric
906 Chemistry Model for Regional and Global Applications, Ph.D. thesis, 250 pp,
907 Virginia Polytechnic Institute and State University, Blacksburg, VA.

908 Zaveri, R. A., R. C. Easter, J. D. Fast, and L. K. Peters (2007), Model for Simulating Aerosol
909 Interactions and Chemistry (MOSAIC), *Journal of Geophysical Research - Atmospheres*,
910 submitted.

911 Zaveri, R. A., R. C. Easter, and L. K. Peters (2005), A computationally efficient
912 Multicomponent Equilibrium Solver for Aerosols (MESA), *Journal of Geophysical*
913 *Research - Atmospheres*, *110*, Art. No. D24203, doi:10.1029/2004JD005618.

914 Zaveri, R. A., R. C. Easter, and A. S. Wexler (2005), A new method for multicomponent
915 activity coefficients of electrolytes in aqueous atmospheric aerosols, *Journal of*
916 *Geophysical Research - Atmospheres*, *110*, Art. No. D02201, doi:10.1029/2004JD004681.

917 Zaveri, R. A., and L. K. Peters (1999), A new lumped structure photochemical mechanism
918 for large-scale applications, *Journal of Geophysical Research - Atmospheres*, *104*, 30387-
919 30415.

920 Zemmelink, H. J., W. W. C. Gieskes, W. Klaassen, H. W. de Groot, H. J. W. de Baar, J. W.
921 H. Dacey, E. J. Hintsa, and W. R. McGillis (2002), Simultaneous use of relaxed eddy
922 accumulation and gradient flux techniques for the measurement of sea-to-air
923 exchange of dimethyl sulphide, *Atmospheric Environment*, *36*, 5709-5717.

924 Zhao, Z., R. E. Stickel, and P. H. Wine (1996), Branching ratios for methyl elimination in the
925 reactions of OD radicals and Cl atoms with CH_3SCH_3, *Chemical Physics Letters*, *251*,
926 59-66.

927 Zhu, L., A. Nenes, P. H. Wine, and J. M. Nicovich (2006), Effects of aqueous organosulfur
928 chemistry on particulate methanesulfonate to non-sea salt sulfate ratios in the marine
929 atmosphere, *Journal of Geophysical Research-Atmospheres*, *111,* Art. No. D05316,
930 doi:10.1029/2005JD006326.

931 Zhu, L., J. M. Nicovich, and P. H. Wine (2003), Temperature-dependent kinetics studies of
932 aqueous phase reactions of hydroxyl radicals with dimethylsulfoxide,
933 dimethylsulfone, and methanesulfonate, *Aquatic Sciences*, *65*, 425-435.

934

935

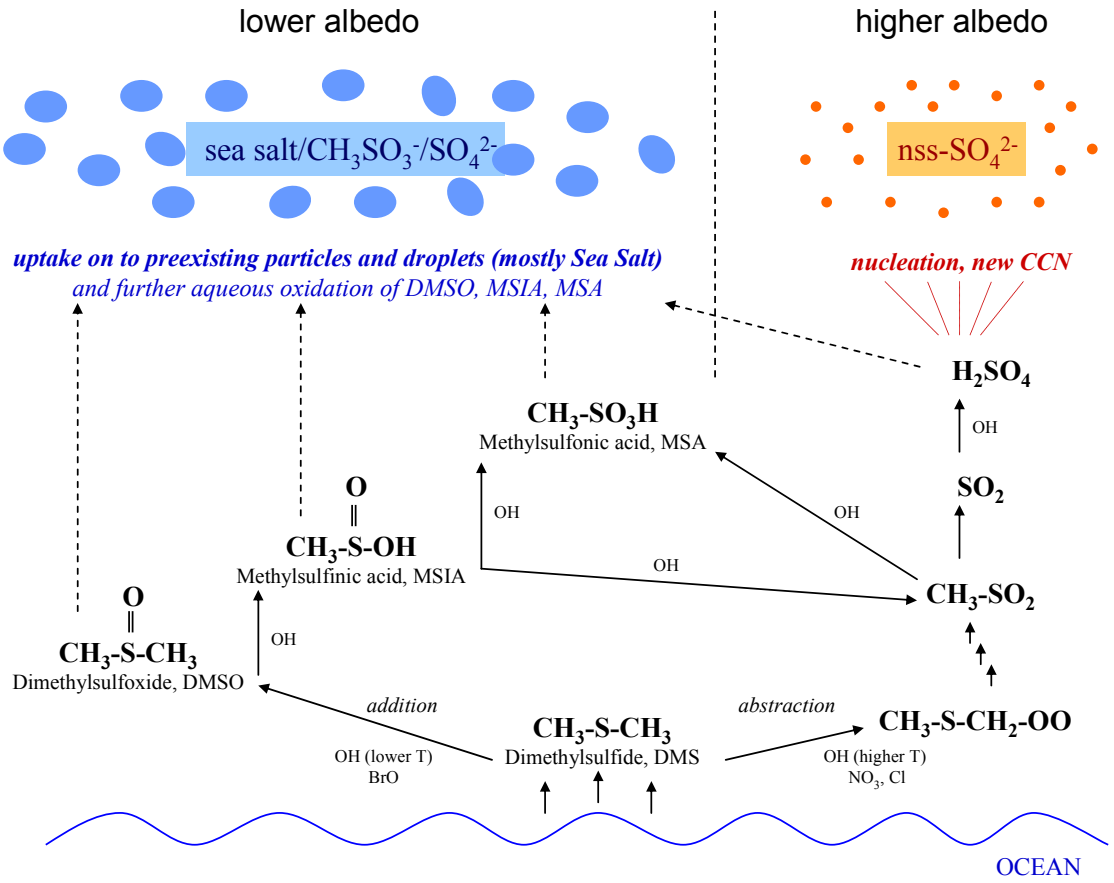

936

937 **Figure 1** Schematic diagram of sulfur-aerosol-climate links in the MBL (adopted from *von*
938 *Glasow and Crutzen*, 2004).

939

940

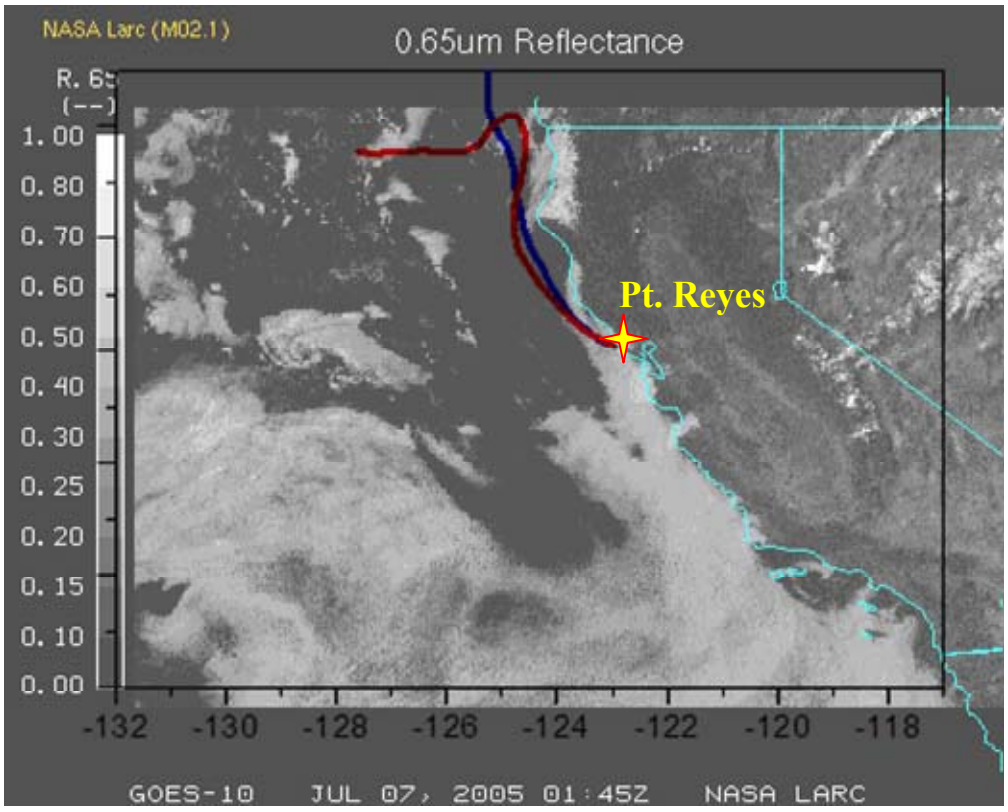

941

942 **Figure 2** GOES-10 satellite image (0.65 micron cloud reflectivity at 4 km resolution) of the
943 California coast, at July 6, 17:45 PST (July 7, 1:45 UTC), showing extensive coastal stratus
944 typical of this region. Superimposed on this image are 48 hour HYSPLIT backtrajectories
945 starting at 10 m AGL on July 6, 21:00 PST (red) and July 7, 09:00 PST (blue)

946

947

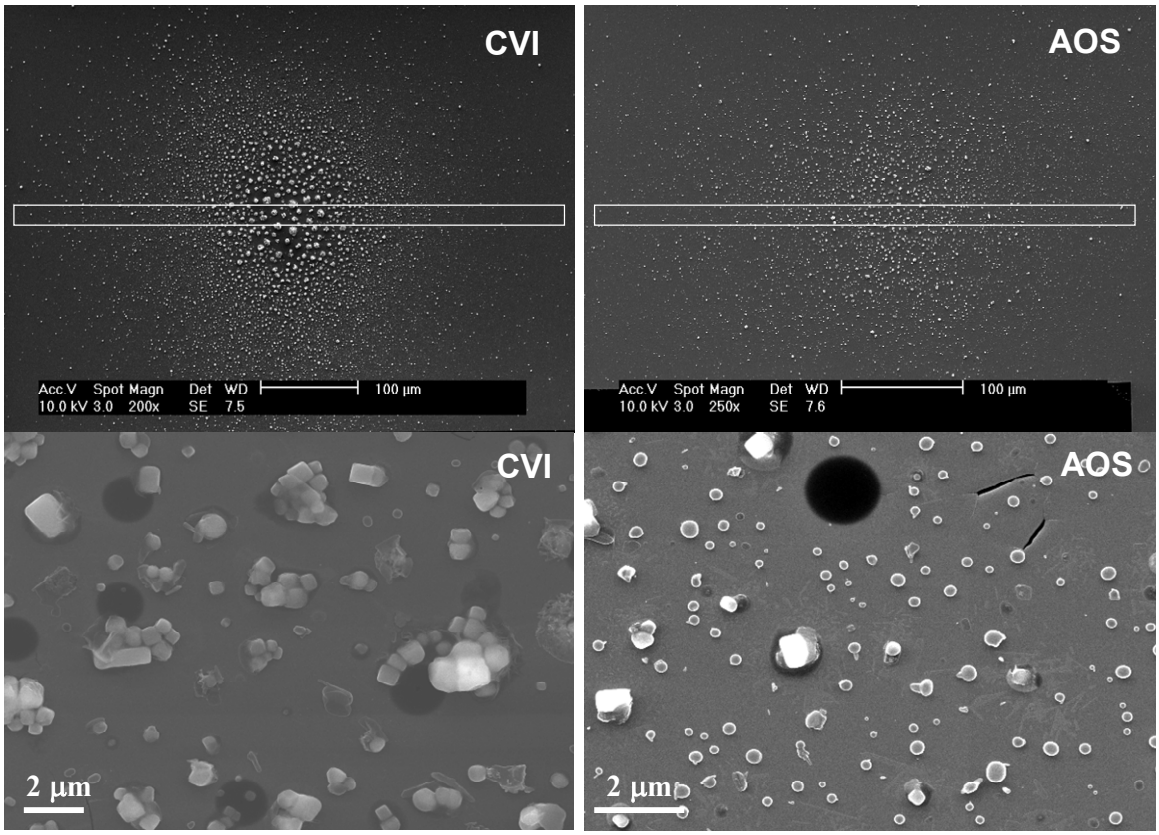

948

949

950

951 **Figure 3** SEM images of two samples collected from the CVI and AOS sampling lines
952 during the cloudy period on July 7, 2005. The upper images are the entire samples and
953 illustrate the spatial inhomogeneity of the deposition spot. Rectangles indicate the regions
954 inspected by CCSEM/EDX analysis. The lower images are magnified fields of view,
955 showing representative particles from the central areas of the samples. Sea salt particles are
956 larger, irregularly shaped supermicron particles with NaCl cubic crystal cores. Ammonium
957 sulfate particles are spherical submicron particles.

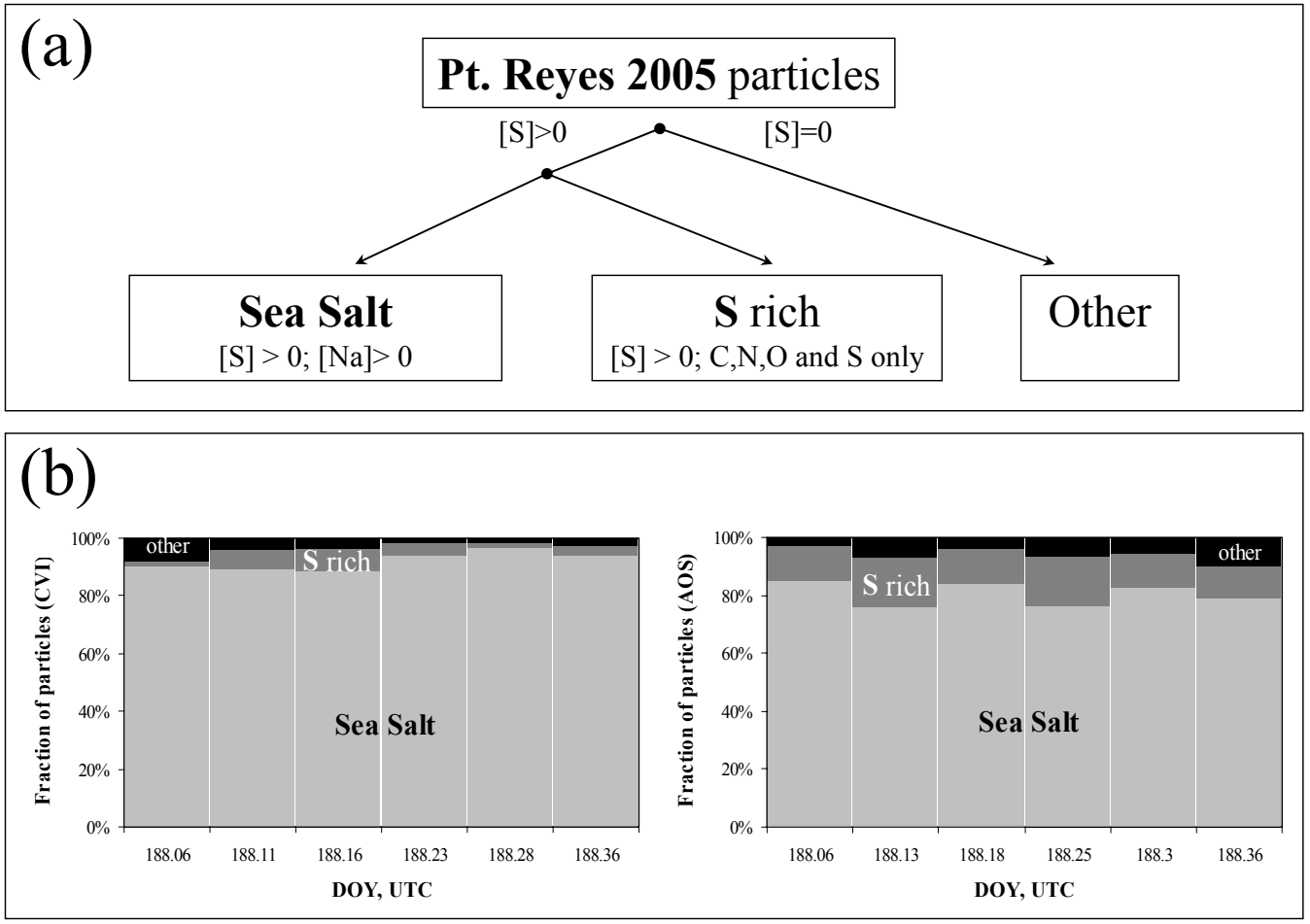

Figure 4 (a) Classification scheme applied to the samples collected during the cloudy period on the night of July 7, 2005 (Point Reyes 2005). (b) Stacked column chart diagram of particle-classes present in the CVI (left panel) and the AOS (right panel) samples.

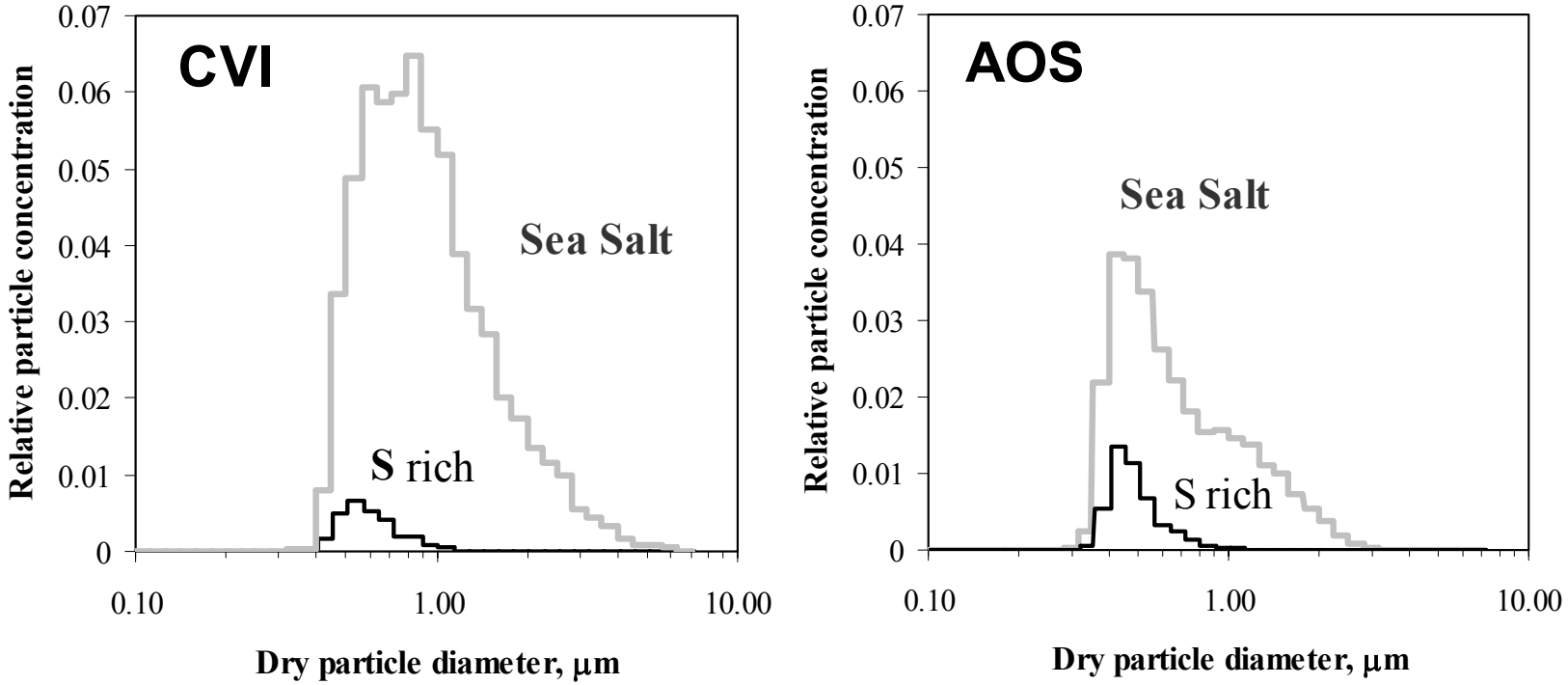

Figure 5 Number distributions of sea salt and S-rich particles in CVI (left panel) and AOS (right panel) samples measured by the CCSEM/EDX analysis. For comparison purposes, all distributions are normalized to the total number of analyzed particles.

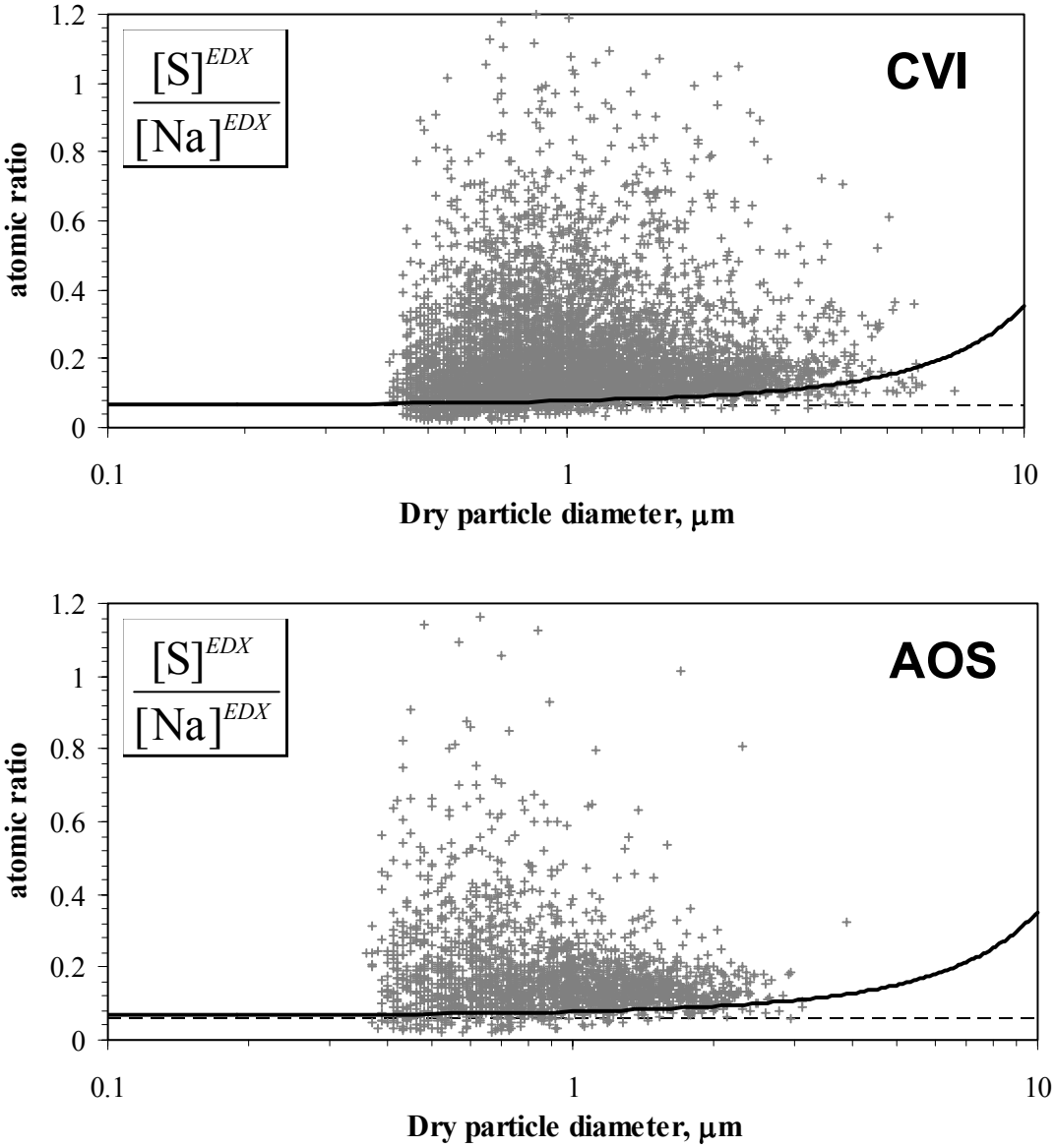

Figure 6 Elemental ratios of S/Na measured by CCSEM/EDX analysis in sea salt particles found in the CVI (upper panel) and the AOS (lower panel) samples. The dashed lines indicate the ratio of 0.06 nominal to sea water. The solid lines indicate expected experimental deviation from the nominal line from sensitivity effects that impact results of EDX particle analysis. See text for further discussion.

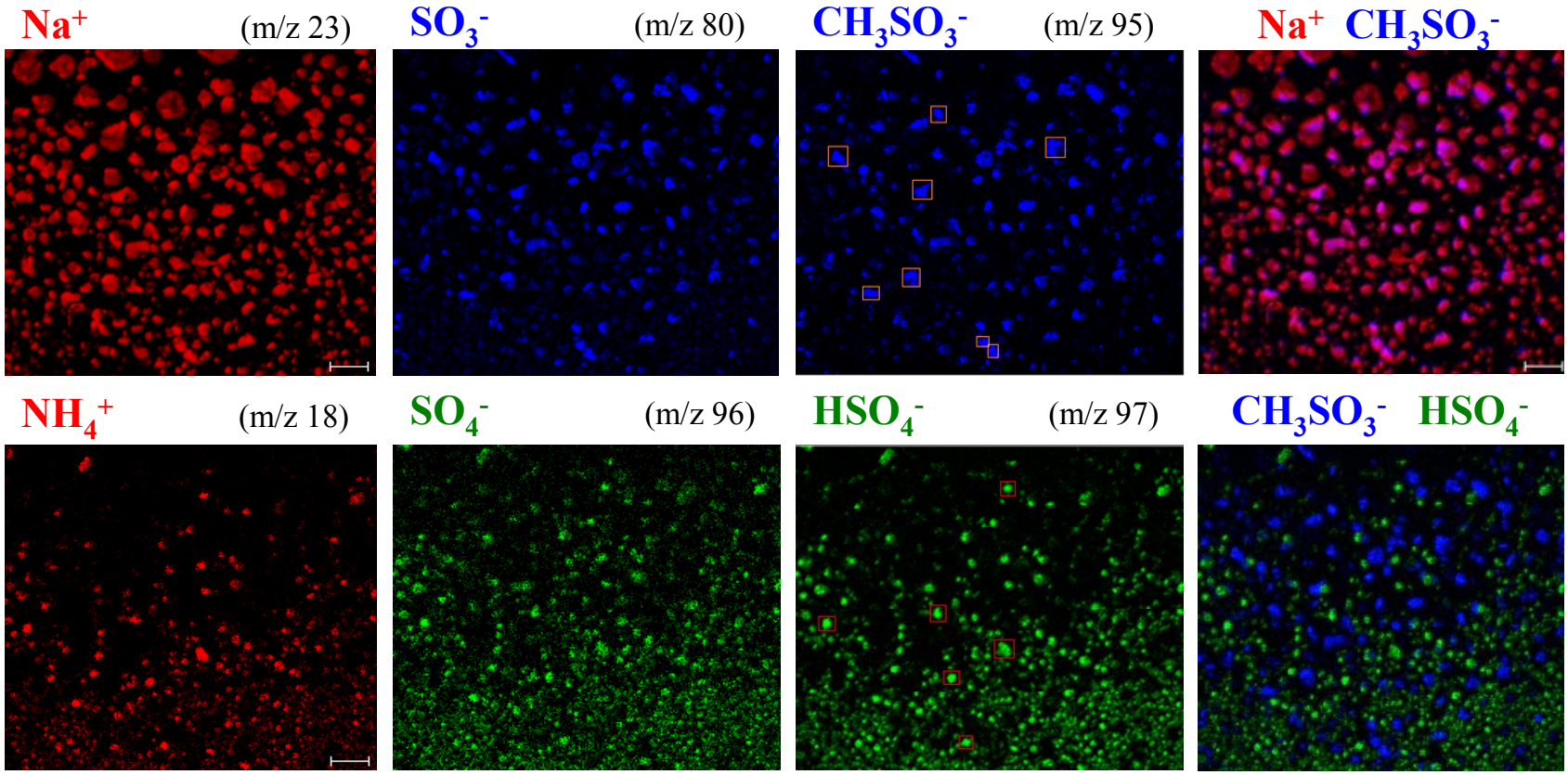

Figure 7 TOF-SIMS maps of typical samples collected from the CVI line. Upper three left images are maps produced for characteristic ions of sodium (Na^+) and methanesulfonate (SO_3^-, $CH_3SO_3^-$). The upper right image shows overlaid maps of the Na^+ and $CH_3SO_3^-$ ions. Their close overlap indicates formation of methanesulfonate in sea salt particles. The lower three left images are maps produced for characteristic ions of ammonia (NH_4^+) and sulfate (SO_4^-, HSO_4^-) originating from $H_2SO_4/(NH_4)_2SO_4$ particles. The lower right image shows overlaid maps of $CH_3SO_3^-$ and HSO_4^- ions and indicates external mixing of sea salt and ammonium sulfate particles. Maps are 100 μm × 100 μm. See text for additional details.

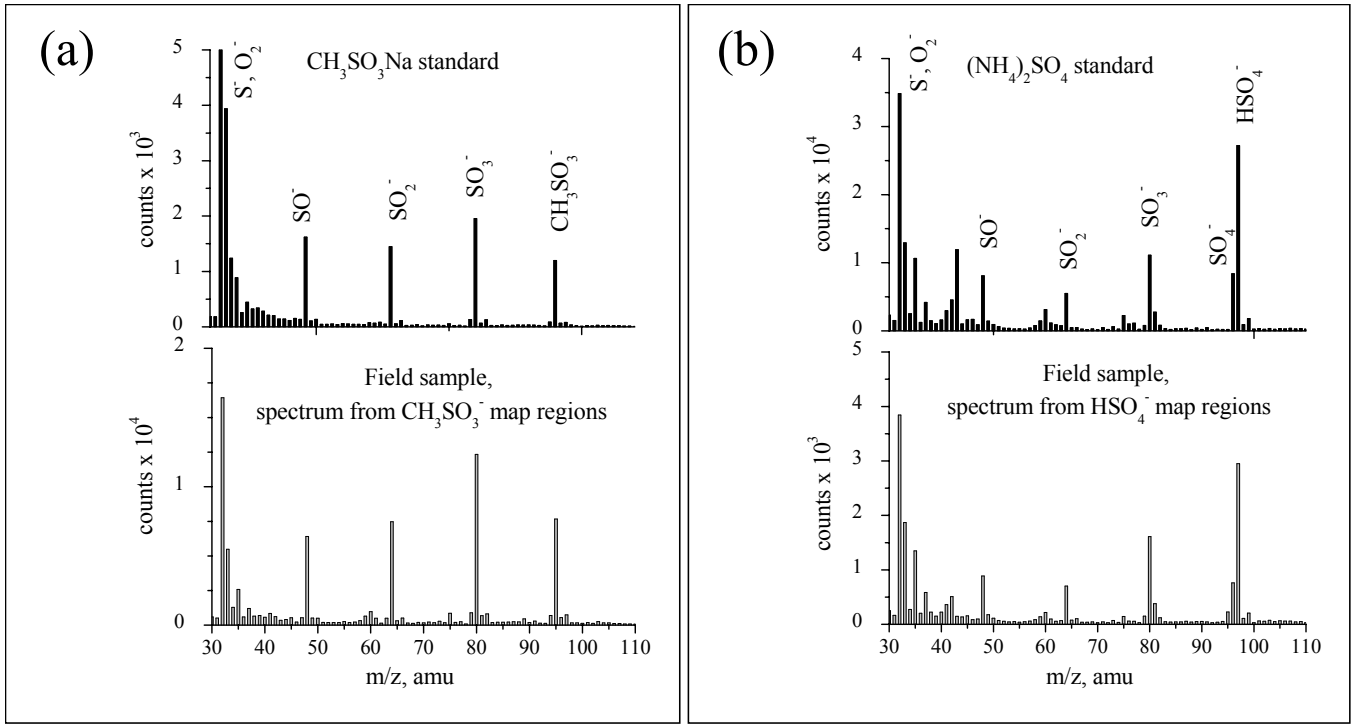

Figure 8 (a) TOF-SIMS spectrum characteristic of sea salt particles (see upper panel of Fig. 7) shown with the reference spectrum obtained from laboratory prepared CH_3SO_3Na particles. (b) TOF-SIMS spectrum characteristic of ammonium sulfate particles (see bottom panel of Fig. 7) plotted along with the reference spectrum obtained from laboratory prepared $(NH_4)_2SO_4$ particles.

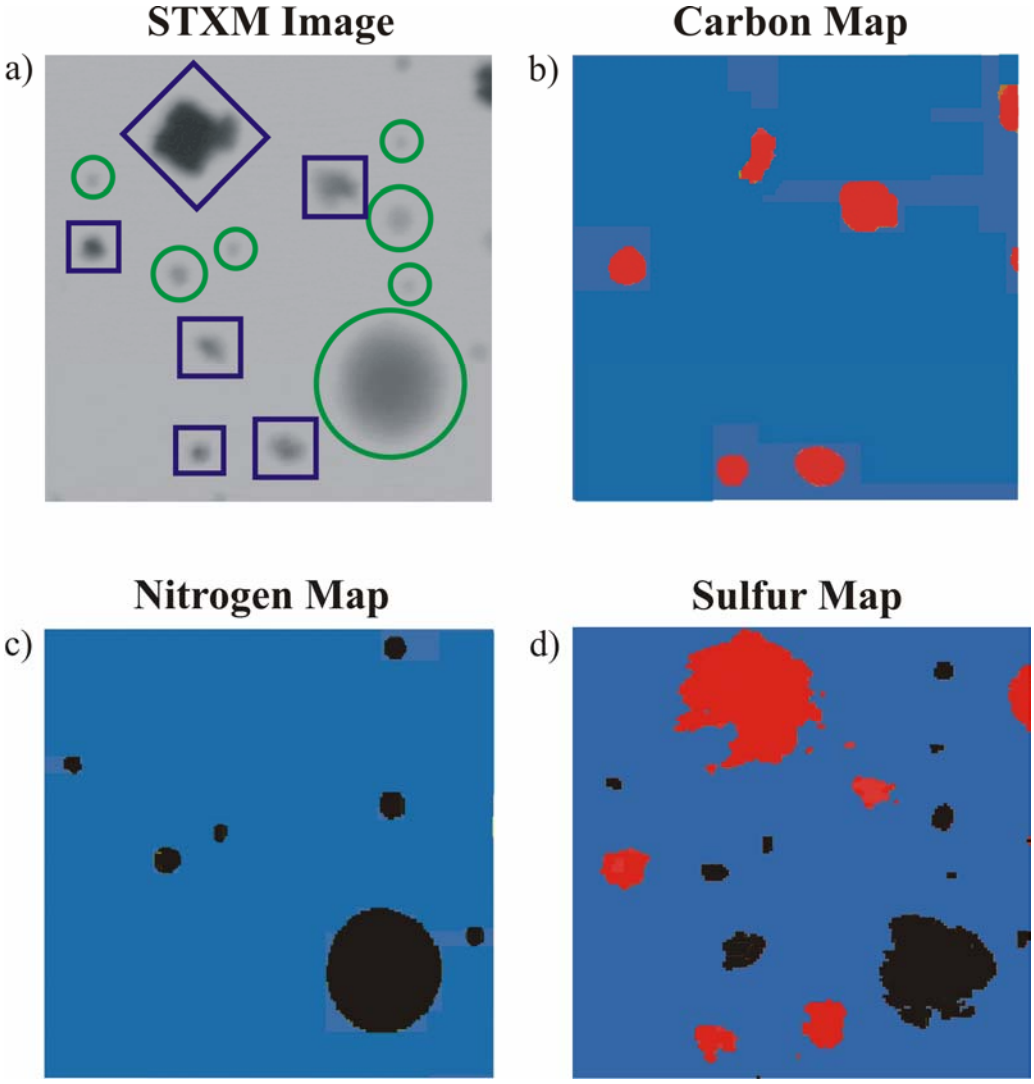

Figure 9 (a) STXM image (12 μm × 12 μm) of externally mixed sea salt/$CH_3SO_3^-$/SO_4^{2-} (marked by squares) and H_2SO_4/$(NH_4)_2SO_4$ (marked by circles) particles, b) C K-edge STXM/NEXAFS map of sea salt/$CH_3SO_3^-$/SO_4^{2-} particles, c) N K-edge STXM/NEXAFS map of H_2SO_4/$(NH_4)_2SO_4$ particles, d) S L-edge STXM/NEXAFS map of sea salt/$CH_3SO_3^-$ /SO_4^{2-} particles (red) and H_2SO_4/$(NH_4)_2SO_4$ particles (black).

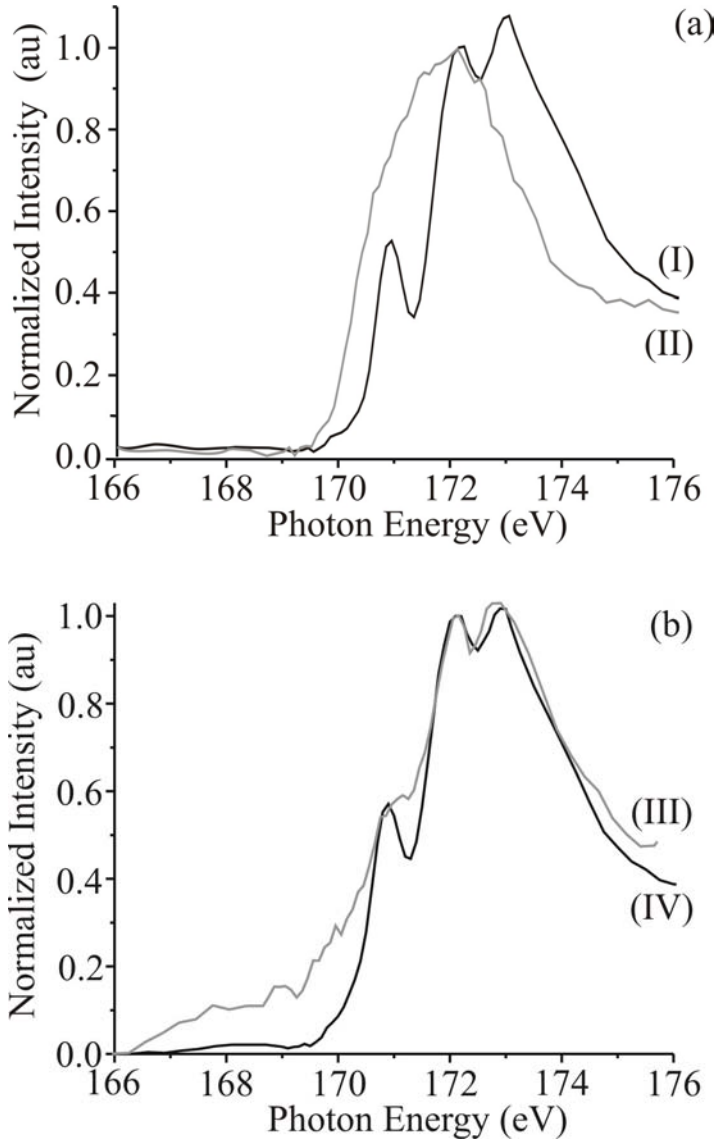

Figure 10 (a) Sulfur L-edge NEXAFS spectra recorded from reference particles of (I) Na_2SO_4 and (II) CH_3SO_3Na. (b) Sulfur L-edge NEXAFS spectrum recorded from a mixed (III) sea salt/$CH_3SO_3^-$/nss-SO_4^{2-} particle collected at Point Reyes National Seashore, (IV) modeled spectrum for 20:80 proportion of CH_3SO_3Na/Na_2SO_4 particle.

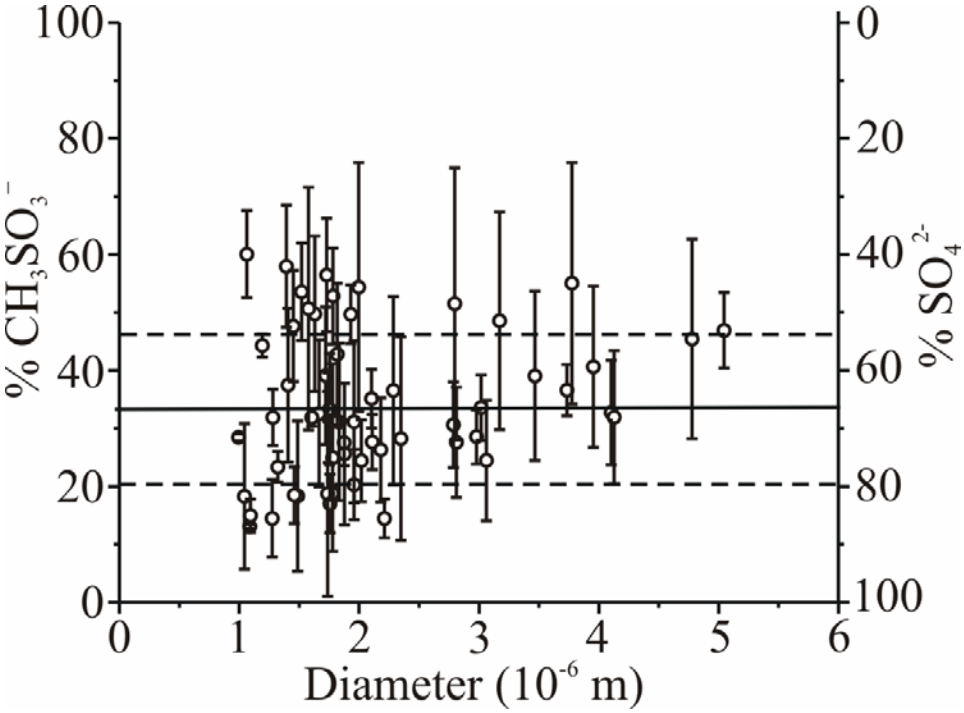

Figure 11 – Invariance in chemical composition with projected particle diameter. The solid black line indicates the mean value of the $CH_3SO_3^-/SO_4^{2-}$ ratio and the dashed lines represent one standard deviation from the mean.

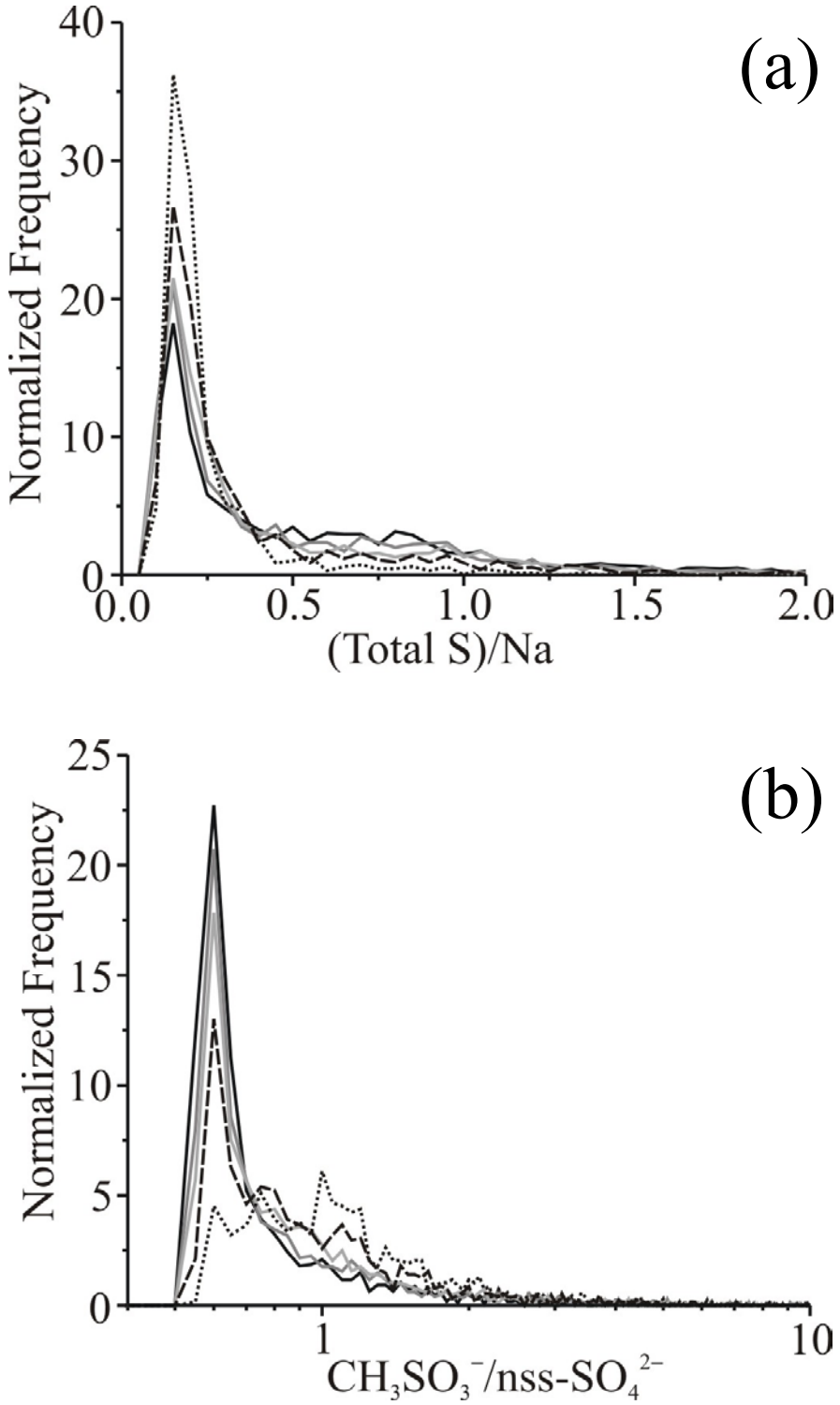

Figure 12 – Distribution of (a) total sulfur to sodium ratio and (b) $CH_3SO_3^-$ to nss-SO_4^{2-} ratio present in particles with diameter in the range 0.31 – 0.5, 0.5 – 0.79, 0.79 – 1.26, 1.26 – 2 and > 2 μm (black, dark grey, light grey, dashed and dotted lines, respectively).

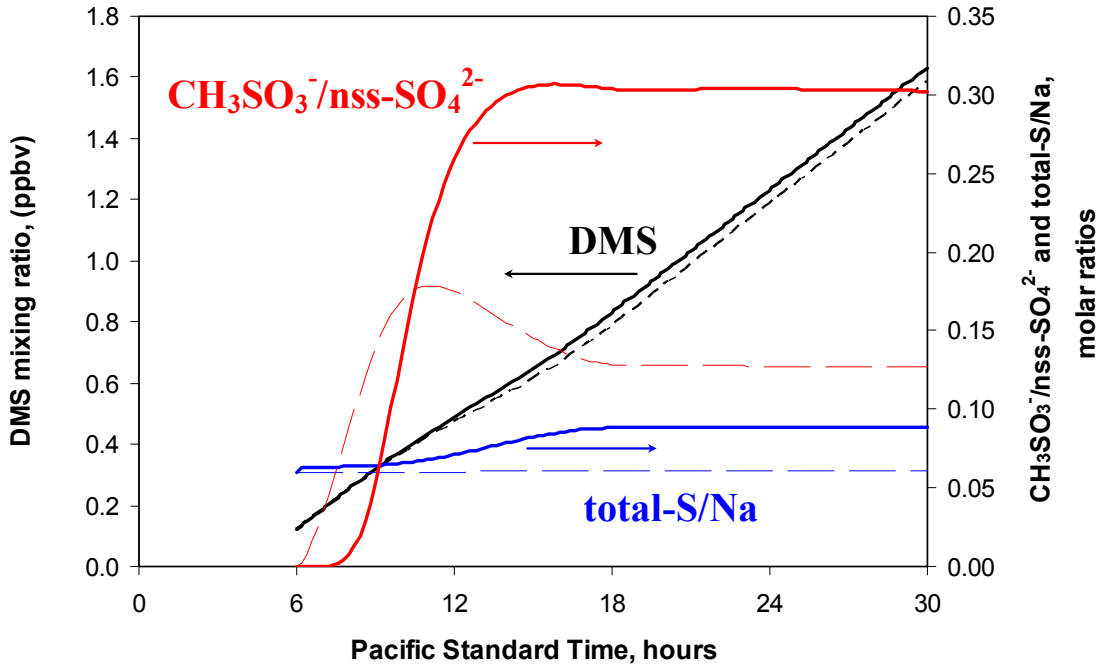

Figure 13 Temporal evolution of $[CH_3SO_3^-]/[\text{nss-}SO_4^{2-}]$ and [total-S]/[Na] ratios in sea salt particles calculated using "gas-phase chemistry only" (dashed lines) and "gas and cloud chemistry" scenarios (solid lines). The model calculations are initiated at 6 am assuming E_{DMS}= 20 μmol·m^{-2}·d^{-1}, emission rates of DMS. Temporal evolution of DMS mixing ratio is also shown.